

Quantifying internal stress and internal resistance associated with thermal ageing and creep in a polycrystalline material

Chen, B. , Hu, J. N. , Flewitt, P. E. J. , Smith, D. J. , Cocks, A. C. F. and Zhang, S. Y.

Author post-print (accepted) deposited in CURVE January 2016

Original citation & hyperlink:

Chen, B. , Hu, J. N. , Flewitt, P. E. J. , Smith, D. J. , Cocks, A. C. F. and Zhang, S. Y. (2014)
Quantifying internal stress and internal resistance associated with thermal ageing and creep
in a polycrystalline material. *Acta Materialia*, volume 67 : 207-219
<http://dx.doi.org/10.1016/j.actamat.2013.12.027>

ISSN 1359-6454

DOI 10.1016/j.actamat.2013.12.027

Copyright © and Moral Rights are retained by the author(s) and/ or other copyright owners. A copy can be downloaded for personal non-commercial research or study, without prior permission or charge. This item cannot be reproduced or quoted extensively from without first obtaining permission in writing from the copyright holder(s). The content must not be changed in any way or sold commercially in any format or medium without the formal permission of the copyright holders.

This document is the author's post-print version, incorporating any revisions agreed during the peer-review process. Some differences between the published version and this version may remain and you are advised to consult the published version if you wish to cite from it.

Quantifying Internal Stress and Internal Resistance associated with Thermal Ageing and Creep in a Polycrystalline Material

B. Chen^{1,a,*}, J.N. Hu^b, P.E.J. Flewitt^c, D.J. Smith^a, A.C.F. Cocks^b, S.Y. Zhang^d

^a*Department of Mechanical Engineering, University of Bristol, Bristol, BS8 1TR, UK*

^b*Department of Engineering Science, University of Oxford, Oxford, OX1 3PJ, UK*

^c*H.H. Wills Physics Laboratory, University of Bristol, Tyndall Avenue, Bristol, BS8 1TL, UK*

^d*ISIS, Science and Technology Facilities Council, Rutherford Appleton Laboratory, Chilton, Didcot, Oxfordshire, OX11 0QX, UK*

*Corresponding author. Tel.: +44 117 331 5941. E-mail: bo.chen-2@manchester.ac.uk

Abstract

In-situ neutron diffraction combined with the incremental deformation at room temperature has been used to provide a measure of the internal stress and internal resistance generated by the prior inelastic deformation at high temperature in an austenitic stainless steel. Interactions between the internal stress and internal resistance are considered explicitly by using the proposed measurement technique. The magnitude of the intergranular internal stress is found to be a function of the total inelastic strain created by high temperature prior deformation. The deviation from linearity observed in the lattice strain response is used to derive the microscopic internal resistance, but a crystal plasticity model is required to infer the absolute value. The macroscopic internal resistance is shown to be consistent with Taylor hardening. A refined internal state concept is proposed based on the Kocks-Mecking model to provide a further step to predict the inelastic deformation.

Keywords: Internal stress; Internal resistance; Crystal plasticity; Neutron diffraction; Creep; Austenitic stainless steel

1. Introduction

When engineering components fabricated from polycrystalline metals and alloys

¹ Present address: Materials Performance Centre, The School of Materials, The University of Manchester, Oxford Road, Manchester, M13 9PL

are subject to extended periods of operation at elevated temperatures, typically greater than 200,000h, there is a potential for the microstructure to change [1, 2]. This can involve for example both rearrangement of the dislocation structure and second-phase precipitation. When precipitation occurs there is usually an associated change in the composition of the matrix. It has been demonstrated that these microstructural changes occurring in Type 316H austenitic stainless steel result in an increased creep deformation rate at a temperature of 823K [3]. In addition, creep deformation results in a change in the material internal state due to variations in the deformation of the differently orientated grains. Here creep deformation is defined as time-dependent inelastic deformation, compared with time-independent inelastic (plastic) deformation. Inelastic deformation leads to the presence of an intergranular internal stress, where the relative strengths of grains determine the magnitudes of the stresses at the length-scale of a grain [4, 5]. There are two significant contributions that lead to changes in material internal state; thermal ageing and prior inelastic deformation. The material internal state manifests itself in many ways; but two that affect deformation rate are (i) a change in the material internal resistance and (ii) the presence of internal stress in particular an intergranular type [6].

The material internal resistance depends on the dislocation density and arrangement and the interactions between the mobile dislocations and other obstacles, such as the presence of solute elements and second-phase precipitates [7-9]. The yield strength of the bulk material depends on these features and can be used to provide a measure of the macroscopic internal resistance. Based on the theory of crystal plasticity applied at the length-scale of a grain, the microscopic internal resistance is related to the critical resolved shear stress (CRSS) on the slip planes [10]. In a polycrystalline material, a grain family consists of several grains which exhibit the equivalently same crystallographic orientation. Various experimental studies [4, 11] have revealed that differently orientated grain families deform different amounts and the deformation is heterogeneous. This heterogeneity creates strain incompatibilities, which lead to the presence of intergranular internal stresses. This type of internal stress may become important when determining the microscopic internal resistance. Also more significant intergranular internal stress may indicate the presence of the macroscopic internal stress in the bulk material. Therefore, the determination of the macroscopic internal resistance may be affected.

The inelastic deformation rate, $\dot{\epsilon}$, is determined by the current state of the material

when the external factors are fixed, for example applied stress, σ_a , and temperature, T , in the case of creep deformation [12]. This leads to a functional description for $\dot{\varepsilon}$:

$$\dot{\varepsilon} = f(\sigma_{op}, T, \sigma_{ir}) \quad (1)$$

where σ_{op} is the operative stress and σ_{ir} is the material internal resistance. The operative stress is defined as a sum of the applied stress, σ_a , and the internal stress, σ_{is} , in the material. Both the internal resistance and internal stress have characteristic length-scales. The presence of the internal stress, σ_{is} , has often not been taken into account when describing the deformation rate [8, 12, 13]; thereby implying that the deformation in a polycrystalline material is homogeneous. This is inconsistent with the experimentally observed feature of heterogeneous deformation that is known to occur in a polycrystalline material [4, 11].

The Kocks-Mecking (KM) model [8, 14, 15], which includes a macroscopic internal resistance term (also called a mechanical threshold stress), has proved to be capable of predicting the creep strain rate of bulk material from its strain hardening behaviour. In this model, the stress-strain curve was related to the transient creep state in a creep test [14]. The KM model follows the general form of equation 1 but with a zero value of macroscopic internal stress. An evolution equation has been proposed in the KM model to describe the change of the macroscopic internal resistance with increasing inelastic strain at given strain rate and temperature, where

$$\frac{d\sigma_{ir}}{d\varepsilon} = g(T, \dot{\varepsilon}, \sigma_{ir}) \quad (2)$$

the strain dependence of the macroscopic internal resistance, σ_{ir} , was considered to be a balance between dislocation accumulation and dynamic recovery [14]. Thus, in a creep test, the strain hardening rate continues to decrease with increasing inelastic strain, i.e. the presence of steady state creep after primary creep. The magnitude of the term σ_{ir} was defined as the yield strength measured at a reference condition, i.e. at a certain temperature and strain rate. This condition can be arbitrarily selected but once chosen remains fixed so that the material internal state and its change with deformation can be characterised. This is done by bringing the material to the

reference condition and measuring the yield strength. Using this concept, Follansbee and Kocks [8] measured the macroscopic internal resistance σ_{ir} by (i) plastically deforming several identical specimens at room temperature and pre-defined strain rate to different levels of inelastic strain; and (ii) reloading each specimen at various temperatures below room temperature to measure the yield strength. This allowed a measure of the term σ_{ir} at a temperature of 0K (reference condition) to be obtained by extrapolation. However, interactions between the macroscopic internal stress and internal resistance were not considered explicitly for this measurement [8].

In the present study, the mechanical threshold stress concept, developed for the KM model, is extended to a length-scale of a grain. The presence of the internal stress created by prior deformation at high temperature is separated from the material internal resistance. The intergranular internal stress is separated from the microscopic internal resistance, whereas the macroscopic internal stress is separated from the macroscopic internal resistance. To achieve this, an experimental approach was developed using in-situ neutron diffraction combined with the incremental deformation at room temperature. Here room temperature is chosen to be the reference condition.

2. Experimental Procedure

Experiments consisted of using specimens of Type 316H stainless steel subjected to prior high temperature deformation and then the internal stresses created by prior deformation measured using neutron diffraction. Incremental room temperature tensile deformation was then applied to the specimens and crystallographic lattice strains were measured using in-situ neutron diffraction during the deformation process. This section describes these details.

2.1. Material

Type 316H austenitic stainless steel, with a chemical composition given in Table 1, was selected. This material had been subjected to 65,015h operation at temperatures between 763K and 803K followed by further thermal ageing at 823K for 22,100h. This is defined as thermally aged material (EXLA). A solution heat treatment at 1363K for 2.5h, followed by water quenching, was applied to the thermally aged

material to produce a solution heat treated (ST) condition. Grain sizes for these two microstructural conditions were measured using the linear intercept method. The averaged grain size for the ST condition was $85\pm 10\mu\text{m}$, and for the EXLA condition was $87\pm 9\mu\text{m}$.

2.2. Prior high temperature deformation

To study systematically the evolution of both the internal stress and internal resistance at two different length-scales associated with the increase in the inelastic strain, both the ST and EXLA specimens were deformed to pre-defined states and unloaded. These states consisted of (i) loading to a stress of 250MPa; (ii) loading plus creep for $\sim 180\text{h}$, (primary creep); (iii) loading plus creep for $\sim 1000\text{h}$, (secondary creep). Specimens without any prior deformation were used to provide the reference state. All prior deformation tests were undertaken at a temperature of 823K and subjected to a tensile stress of 250MPa. Uniaxial round bar specimens with a 28.25mm gauge length and 5.65mm diameter were used to conduct the tests. During all tests, two linear variable differential transducers (LVDTs) were used to measure the elongation of each specimen.

Table 2 summarises all the specimens together with their prior deformation histories. Specimens 1 (1A, 1B, 1C) to 4 were extracted from the ST material. Specimens 5 to 8 were extracted from the EXLA material. The left hand side in Figure 1 (a) shows the strain history for a typical specimen; in this case strained to reach primary creep. The specimen was heated to the test temperature of 823K, step 1 in Figure 1 (a). This was followed by applying an external load to the specimen, to reach a stress of 250MPa, step 2 in Figure 1 (a). Time-independent inelastic strain, i.e. plastic strain, was introduced to the specimen during step 2. After loading, the specimen was then creep deformed to the pre-defined test duration of 180h, step 3 in Figure 1 (a). This was followed by cooling at the applied stress to retain the high temperature deformation induced dislocation structure. Finally the specimen was unloaded elastically and dismantled at room temperature. This procedure was applied to all prior deformed specimens shown in Table 2.

2.3. Measurements of intergranular and macroscopic internal stress

The specimens were then measured using neutron diffraction. The arrangement of a specimen in the ENGIN-X neutron diffractometer is shown in Figure 2, where the diffracted neutron beams were collected by two detectors: detector 1 for the axial diffraction vector and detector 2 for the radial diffraction vector. The applied stress direction for the prior high temperature deformation was parallel to the axial diffraction vector. Since the ENGIN-X neutron diffractometer is based on the concept of time-of-flight, many diffraction peaks corresponding to different grain families were measured simultaneously [16]. Four main diffraction peaks were considered: $\{111\}$, $\{200\}$, $\{220\}$ and $\{311\}$. A single peak fitting routine, available at ENGIN-X, was used to determine the lattice spacing [16]. This provides a measure of intergranular internal strain corresponding to each individual diffraction peak. A 3mm×3mm×4mm gauge volume was used for the neutron diffraction measurements to ensure that the sampled gauge volume was fully contained within the specimen, as illustrated in Figure 2. A typical measurement time of 540s was selected to ensure good counting statistics for the diffraction peaks.

Intergranular internal stresses due to the prior deformation at high temperature were quantified from the change in the lattice spacing for each individual peak. It was assumed that specimens 1 (1A, 1B, 1C) and specimen 5, Table 2, contained no intergranular internal stresses since they had been subjected to no prior deformation. The lattice spacing measured in specimens 2 to 4 and 6 to 8, Table 2, was then compared with that measured in specimens 1A and 5, respectively. The intergranular internal strain was then derived from the change in the measured lattice spacing:

$$\varepsilon_{hkl}^i = \frac{d_{hkl}^i - d_{hkl}^0}{d_{hkl}^0} \quad (3)$$

where ε_{hkl}^i is the intergranular internal strain in specimen i ($i=2$ to 4 and 6 to 8 based on Table 2), measured from a specific crystallographic plane $\{hkl\}$. d_{hkl}^i is the lattice spacing in a $\{hkl\}$ grain family measured from specimen i . d_{hkl}^0 is the stress free lattice spacing from specimens 1A and 5 for the ST and EXLA specimens, respectively. Knowing the axial strain and radial strain in each specimen measured

from detectors 1 and 2, as shown in Figure 2, the intergranular internal stress along the axial direction was then derived from the measured strain vectors using the generalised Hooke's law:

$$\sigma_{hkl}^{i,zz} = \frac{E_{hkl}}{1+\nu} \varepsilon_{hkl}^{i,zz} + \frac{E_{hkl}\nu}{(1+\nu)(1-2\nu)} (\varepsilon_{hkl}^{i,zz} + \varepsilon_{hkl}^{i,\theta\theta} + \varepsilon_{hkl}^{i,rr}) \quad (4)$$

where $\sigma_{hkl}^{i,zz}$ is the axial stress vector measured in specimen i . E_{hkl} is the diffraction elastic constant for the $\{hkl\}$ grain family and ν is the Poisson's ratio ($\nu=0.29$). The diffraction elastic constants (DECs) for all four grain families were determined from the neutron diffraction measurements during in-situ loading in the elastic region. This will be described later. $\varepsilon_{hkl}^{i,zz}$, $\varepsilon_{hkl}^{i,\theta\theta}$ and $\varepsilon_{hkl}^{i,rr}$ are axial, hoop and radial strain vectors, where the three superscripts, zz , $\theta\theta$ and rr , are three principal directions in the cylindrical coordinate system. For the present neutron diffraction measurement, only the internal stress state at the centre of the specimen was required, thus the measured lattice strain along the radial direction is equal to that along the hoop direction ($\varepsilon_{hkl}^{i,rr} = \varepsilon_{hkl}^{i,\theta\theta}$).

In the ENGIN-X time-of-flight instrument, the macroscopic internal strain can be approximated from the change in the average lattice parameter by adopting a Rietveld refinement analysis applied to the complete diffraction spectrum [17]. The macroscopic internal stress in the bulk material was derived from this macroscopic strain [17] using a Young's modulus of 210GPa and a Poisson's ratio of 0.29. This is instead of using the specific crystallographic diffraction elastic constants shown in equations 3 and 4, which have been adopted for a single peak analysis.

2.4. Incremental tensile deformation combined with neutron diffraction

Each of the prior deformed specimens was subjected to incremental tensile deformation at room temperature combined with the neutron diffraction measurements, Figure 1. The incremental tensile deformation tests were undertaken at a constant strain rate of $5 \times 10^{-6} \text{s}^{-1}$ using a 100kN servo-hydraulic test rig in the ENGIN-X neutron diffractometer. An extensometer was attached to each specimen to

measure the macroscopic strain applied to the material. The right hand side of Figure 1 (a) shows the strain history applied to a representative specimen at room temperature. Figure 1 (b) shows the applied stress history during the incremental tensile deformation, where the stress level was increased step by step to enhance the accuracy for the determination of the yield strength.

During in-situ loading the specimens were measured using the ENGIN-X neutron diffractometer as shown in Figure 2. Four diffraction peaks were measured using the same gauge volume as described in section 2.3. At the end of each loading step, Figure 1 (b), the specimen was held at either a constant stress (elastic region) or at a constant strain (plastic region) for the period of the measurement. Some stress relaxation was observed when the stress was higher than 300MPa, Figure 1 (b). To ensure this stress change was less than 3MPa when a measurement was undertaken in the plastic region, a pre-defined delay for starting the measurement, ranging from 180s to 360s, was adopted. Therefore, all the neutron diffraction measurements were undertaken at a constant stress. The unloading step (at ~5MPa), as shown in Figure 1 (b), was used to measure the residual elastic lattice strain from each grain family. The macroscopic plastic strain was measured by the attached extensometer for the unloaded step. In this paper, we present neutron diffraction measurement results obtained during in-situ loading.

The evaluation of elastic lattice strain in each grain family during the in-situ loading required a measure of the lattice spacing under a stress free condition. The elastic lattice strain was determined from a change in the lattice spacing, compared with the measured lattice spacing before applying the in-situ loading to the specimen. The latter provided the stress free lattice spacing for this case to calculate the elastic lattice strain based on equation 3. Thus each specimen shown in Table 2 had a different value of lattice spacing appropriate to each grain family measured before applying in-situ loading to the specimen.

2.5. Measurements of microscopic and macroscopic internal resistance

The deviation from linearity measured in each grain family provided a measure of microscopic internal resistance representative of that grain family. The magnitude of microscopic internal resistance was assumed to be related to the applied stress required to produce the onset of the deviation from linearity when the measured

elastic lattice strain was plotted against the applied stress. The yield strength was determined from the stress-strain relationship for each specimen and these data provided a measure of the macroscopic internal resistance. Primarily based on the resolution of extensometer, a strain offset of 0.01% together with the Young's modulus was employed to determine the macroscopic internal resistance. Both the microscopic and macroscopic internal resistances measured using the methods described above took no account of the presence of intergranular and macroscopic internal stresses, respectively. The separation of the internal stress from the determined internal resistance will be explained later.

3. Results

The results derived from the measurements are examined in this section. First, the prior high temperature deformation is evaluated together with the macroscopic and intergranular internal stresses. Second, a measure of the macroscopic internal resistance was determined by using a strain offset of 0.01% together with the Young's modulus for each specimen. Macroscopic internal stress, estimated by Rietveld refinement analysis, was then separated from the determined macroscopic internal resistance. Third, the measured lattice strains derived during in-situ loading are presented in terms of the deviation from linearity. The applied stress required to create the onset of deviation from linearity was determined. This provided a measure of the microscopic internal resistance. Finally, the separation of the intergranular internal stress from the determined microscopic internal resistance is presented in this section.

3.1. Prior high temperature deformation and internal stresses

Table 2 summarises the magnitude of the inelastic strain accumulated by prior deformation at a temperature of 823K for all specimens. For ST specimens 2 to 4, the inelastic strain accumulated from loading was much higher than that from creep deformation. A true strain of 5.76% was obtained from the loading, compared to that of 1.26% from subsequent creep for 1000h, specimen 4 in Table 2. However, for EXLA specimens 6 to 8, the inelastic strain accumulated from loading was smaller than that from creep deformation. An inelastic strain of 4.86% was introduced by

creep for 1000h in specimen 8, compared to an inelastic strain of 1.98% from the loading, Table 2. Figure 3 (a) shows the stress-strain relationship obtained during loading of specimens 4 (ST) and 8 (EXLA). A higher inelastic strain was introduced by loading specimen 4 to 250MPa compared with that observed in specimen 8. Figure 3 (b) shows the temporal changes in both the true stress and true strain during the creep tests for specimens 4 (ST) and 8 (EXLA), which were subjected to creep for 1000h (secondary creep). There was an insignificant increase in the true stress and true strain with increasing creep time in the ST specimen, compared with EXLA specimen. Thus ST specimens had a higher resistance to creep deformation, but a lower resistance to plastic deformation induced by loading.

Figure 4 shows the derived axial internal stresses created as a result of high temperature deformation for both ST and EXLA specimens summarised in Table 2. The internal stresses are shown as a function of the total inelastic true strain accumulated by prior straining, which is the sum of plastic and creep strains, as illustrated in Table 2. In general, an increase in the magnitude of the prior strain led to a higher magnitude of internal stress, Figure 4. Intergranular internal stresses in the {200} grain family were tensile, whereas in the {220} grain family were compressive, Figure 4. Rietveld refinement analysis gave almost zero values of macroscopic internal stresses, except for the specimens subjected to an inelastic strain of greater than 5%, Figure 4. The magnitudes of the internal stresses were similar for specimens 2 and 3 in Figure 4. This is consistent with the small difference in the total inelastic strain in these two specimens, Table 2.

3.2. Macroscopic internal resistance

Figure 5 shows the macroscopic stress-strain relationship obtained during in-situ loading of specimen 1A. The macroscopic Young's modulus of 205GPa was obtained from the slope between the applied stress and extensometer measured macroscopic strain. This is shown in Figure 5 together with a strain offset of 0.01%, where the determined macroscopic internal resistance in specimen 1A was obtained to be 128MPa. The macroscopic internal resistance in each specimen shown in Table 2 was determined using the same method. The results are summarised in Table 3. Also shown in this table is the corrected value of macroscopic internal resistance for each specimen by considering the macroscopic internal stress. The macroscopic internal

stress for each specimen was obtained by the Rietveld refinement, Figure 4. Prior loading resulted in a higher magnitude of internal resistance, 345MPa for specimen 6 compared to the no loading condition, 177MPa for specimen 5, Table 3. However, secondary creep decreased the macroscopic internal resistance to 283MPa for specimen 8. The highest value of the macroscopic internal resistance was observed in the primary creep deformed specimen 7, Table 3. For ST specimens, there was little difference in the corrected macroscopic internal resistance from specimens 2 to 4 subjected to a loaded, primary creep and secondary creep, respectively. This is consistent with the small change in the true stress measured over the period of creep, see specimen 4 in Figure 3 (b).

3.3. Lattice strains and deviations from linearity during room temperature deformation

Figures 6 (a) and (b) show neutron diffraction measured elastic lattice strains along the axial direction during in-situ loading for specimens 1A to 1C. Specimen 1B and 1C were deformed to an applied stress less than 170MPa, as shown in Figures 6 (a) and (b). There is a good agreement between measured lattice strains from all four grain families in these three specimens.

Diffraction elastic constants (DECs) were determined through a linear least square fit to the measured lattice strain as a function of the applied stress within the elastic region of in-situ loading. DECs in the $\{220\}$ and the $\{200\}$ grain families were found to be $E_{220}=207\pm11\text{GPa}$ and $E_{200}=156\pm3\text{GPa}$, respectively. They are the stiffest and the most compliant among the four grain families, see Table 4. After comparing all specimens, the effect of the prior deformation or the thermal ageing on the DECs is found to be insignificant. The uncertainty was determined by the standard deviation (STDEV) when the linear least square fitting was used within the elastic region of in-situ loading. These DECs are in good agreement with previous values given by Clausen et al. [4].

The elastic lattice strains based on the derived DECs for the $\{200\}$, $\{220\}$, $\{111\}$ and the $\{311\}$ grain families are illustrated in Figures 6 (a) and (b) for specimens 1A to 1C. By comparing these with measured elastic lattice strains, the onset of deviation from linearity can be seen for the $\{200\}$ and the $\{220\}$ grain families. The onset of deviation from linearity is consistent with the determined macroscopic internal resistance for specimen 1A, as indicated in Figure 6 (a). The deviation from linearity

for each grain family was calculated from the difference between the measured elastic lattice strain and the expected linear lattice strain by DEC's. The measured elastic lattice strain in the $\{220\}$ grain family became smaller than the expected linear lattice strain, Figure 6 (a). It is the onset of the deviation from linearity that is related to the yielding of grains belonging to a particular grain family. In this case, yielding occurred in some grains belonging to the $\{220\}$ grain family. This will be discussed later with respect to a newly developed crystal plasticity model. As a consequence, the $\{200\}$ grain family exhibited a higher value of measured lattice strain compared with the expected one, Figure 6 (a). This indicates the effects of sharing load due to the yielding of some grains belonging to another grain family. The magnitudes of the deviations from linearity in these two grain families $\{220\}$ and $\{200\}$ increased with increasing applied stress during in-situ loading, Figure 6 (a), where a negative value occurred in the $\{220\}$ grain family and a positive value occurred in the $\{200\}$ grain family. Both $\{111\}$ and $\{311\}$ grain families showed little deviation from linearity at applied stresses that were higher than the macroscopic internal resistance, Figure 6 (b).

By comparing the responses of ST specimen 1A and EXLA specimen 5, the influence of thermal ageing on the response of measured lattice strain as a function of applied stress is shown in Figure 7 for both the $\{200\}$ and $\{220\}$ grain families. Thermal ageing resulted in a higher value of applied stress being required to produce an onset of the deviation from linearity. The difference was found to be $\sim 30\text{MPa}$. These data were compared with a model prediction, see the solid and dotted lines in Figure 7. A crystal plasticity model was developed from our previous work [18] and this will be described later. By using an initial value of critical resolved shear stress (CRSS) of 68MPa for ST condition and 80MPa for EXLA condition, the predicted onset of deviation from linearity is consistent with the present measurement, Figure 7. In earlier work by Daymond and Bouchard [11] and Clausen et al. [4], values of CRSS for stainless steel equal to 68MPa and 87MPa respectively were used to obtain the best fit between the in-situ experiment and model.

The deviations from linearity in the $\{220\}$ grain family during in-situ loadings of ST specimens and EXLA specimens are shown in Figures 8 (a) and (b), respectively. The uncertainties shown here are related to the determination of DEC's as given in Table 4. This applies to all figures regarding the deviations from linearity in this paper. A second order least square regression fit was adopted to give a general trend of the changes in each specimen. For the ST condition, high negative values of the

deviation from linearity in the {220} grain family were observed in specimens 1 (1A, 1B, 1C) and 3, Figure 8 (a). The former experienced no prior deformation and the latter was subjected to primary creep prior deformation, Table 2. Little deviation from linearity in the {220} grain family was observed in specimens 2 and 4, and curves were not fitted to data shown in Figure 8 (a) for these two specimens. For the EXLA specimens, specimen 5 (no loading) showed the highest magnitude of the deviation from linearity among the four, Figure 8 (b). Specimen 8 showed a different lattice strain response, where only limited deviation from linearity was observed at an applied stress of ~ 400 MPa in Figure 8 (b). Large variations in the deviation from linearity occurred in the whole elastic region during the in-situ loading for specimen 8.

Figures 9 (a) and (b) show the onset of deviation from linearity observed in the {200} grain families for ST and EXLA specimens, respectively. For the ST condition, high positive values of the deviation from linearity were observed in specimens 1 (1A, 1B, 1C). There was a deviation from linearity in specimen 2 (positive value), but the magnitude was limited, Figure 9 (a). For specimen 4, the {200} grain family exhibited a negative value of deviation from linearity. This indicates that the occurrence of yielding in some grains belonging to the {200} grain family for specimen 4. For the EXLA condition, all specimens showed certain levels of deviations from linearity in the {200} grain family, except for specimen 7, Figure 9 (b).

Except for ST specimen 2, all other specimens exhibited different amounts of negative deviation from linearity in some grain families, the {220} grain family for six specimens (1, 3 and 5 to 8) in Figures 8 (a) and (b) as well as the {200} grain family for ST specimen 4 in Figure 9 (a). We examined all four grain families contributing to diffraction intensity for ST specimen 2. However, none of the grain families exhibited a negative deviation, but there was a positive deviation for the {200} grain family, Figure 9 (a). This indicates that some grains yielded and the {200} grain family shared the loading. Thus it is likely that those yielded grains did not contribute to diffraction intensity significantly.

3.4. Microscopic internal resistance

The onset of the deviation from linearity in each specimen was evaluated by using a fixed deviation value of 100×10^6 . This provided a measure of microscopic internal

resistance within the selected grain families; both the $\{220\}$ and the $\{200\}$ grain families. When determining the microscopic internal resistance from the observed deviation from linearity, as shown in Figures 8 (a) and (b) for the $\{220\}$ grain family, the presence of the intergranular internal stress needs to be taken into account. As shown in Figure 4, compressive intergranular internal stresses were present in the $\{220\}$ grain family for those prior deformed specimens.

Figure 10 illustrates the method used to determine the microscopic internal resistance in two typical specimens 5 and 8. Figure 10 (a) shows the deviation from linearity in the $\{220\}$ grain family for EXLA specimens 5 and 8, as a function of the sum of the applied true stress and the intergranular internal stress. The curves obtained from second order regression fits, as previously shown in Figure 8 (b), are shown in Figure 10 (a). The origin for specimen 8 has been shifted to the left due to the presence of a compressive internal stress in the $\{220\}$ grain family resulting from prior deformation, see Figure 4. Thus the microscopic internal resistance in the $\{220\}$ grain family was obtained to be 218MPa for specimen 5 and 230MPa for specimen 8, Figure 10 (a). Figure 10 (b) shows the deviation from linearity in the $\{200\}$ grain family for EXLA specimens 5 and 8. The origin of specimen 8 has been shifted to the right in Figure 10 (b), due to the presence of a tensile intergranular internal stress in the $\{200\}$ grain family, Figure 4. Thus the microscopic internal resistance in the $\{200\}$ grain family was obtained to be 172MPa for specimen 5 and 385MPa for specimen 8, Figure 10 (b).

The same method described above was adopted to determine the microscopic internal resistance in all specimens. The determined microscopic internal resistances are summarised in Table 5. The presence of the intergranular internal stress in these two grain families were taken into account for the results given in Table 5. First, there were no deviations from linearity (less than the fixed deviation value of 100×10^6) in the $\{220\}$ grain family for ST specimens 2 and 4, in the $\{200\}$ grain family for ST specimen 3 and in the $\{220\}$ grain family of EXLA specimen 7. This is consistent with the features observed in Figures 8 and 9. Second, the microscopic internal resistances in the $\{220\}$ grain family of EXLA specimens were similar, except for EXLA specimen 7. ST specimen 3 also had a lower value of microscopic internal resistance in the $\{220\}$ grain family compared with ST specimen 1. Both specimens 3 and 7 were subjected to prior primary creep. For the $\{200\}$ grain family, high magnitudes of microscopic internal resistances were obtained in all prior deformed

specimens.

4. Discussion

4.1. Creation of intergranular internal stress

In a global homogeneous polycrystalline material, individual grains are constrained by surrounding grains when subjected to an externally applied stress. The mechanical response of each grain must adapt to its neighbours which, in general, are composed of an arrangement of several differently orientated grains. The internal stress developed between the grains arises from interaction between a given grain and those surrounding [5]. The magnitude of this stress in a given grain will be determined by the relative strength and orientation of the neighbours. Figure 11 is a simplified 2-D schematic diagram that can be used to explain the 3-D response of the polycrystals when subjected to an externally applied load. Here three individual grains (grains 1, 2 and 3) are assigned the same crystallographic orientation, illustrated by the same colour. Each grain is surrounded by differently orientated grains (polycrystals I, II and III), which form a locally heterogeneous environment for the grain of interest, Figure 11. When an external stress, σ_a , is applied uniformly to the globally homogeneous polycrystal, the characteristics of the most immediate neighbouring grains can have a pronounced impact on the stress-strain state experienced by the grain of interest. An externally applied stress creates an inelastic strain in the grain of interest and the neighbouring grains. When unloaded an internal stress created by the misfit strain is retained. The magnitude of the stress depends on the relative strength of the most immediate neighbouring grains. Thus the stress-strain state for grains 1, 2 and 3, Figure 11, will be different although in this case they have the same idealised crystallographic orientation.

If we consider the stress-strain behaviour of a group of grains exhibiting the equivalently same crystallographic orientation, such as grains 1 to 7 illustrated in Figure 11, or even a larger group, the average behaviour of these grains with a specific crystallographic orientation will be obtained. In addition, each grain has its own characteristic stress-strain state and this creates a variation at the length-scale of a grain. We may visualise each colour shown in Figure 11 for the polycrystals to represent a particular grain family, such as the $\{220\}$, $\{200\}$, $\{111\}$ and $\{311\}$ grain

families considered in this paper. The elastic lattice strain response to the applied stress in various grain families in a polycrystalline material was studied earlier both experimentally and through a self-consistent model [4, 19, 20]. However, it is essential to recognise that the models do not take into account the grain-to-grain variation.

4.2. In-situ neutron diffraction measurement and crystal plasticity model

Neutron diffraction measures the lattice spacing of several similarly orientated grains within the sampled gauge volume, Figure 2. This provides an average value over several grains; each of them having experienced different stress-strain state. A simple calculation based on a 3mm×3mm×4mm gauge volume and a typical grain size of 90µm gives a total of ~49,400 grains within the measured gauge volume. Due to the inherently selective characteristics of the neutron diffraction technique, the individual response of different grain families will be measured simultaneously by using the ENGIN-X neutron diffractometer. As demonstrated by the measured elastic lattice strains in specimen 1 (1A, 1B, 1C), which received no prior deformation, high reproducibility is obtained, Figure 6. Specimen 8, subjected to prior secondary creep deformation of 6.8%, exhibited a large variation in the measured elastic lattice strain of the {220} grain family, illustrated by the calculated deviation from linearity in Figure 8 (b), when an external stress is applied to the material. This large variation in the {220} grain family indicates that different grains belonging to this grain family yielded at different applied stresses depending on the magnitude of the pre-existing intergranular internal stress. These grains exhibit a similar diffracting plane orientation and thereby contribute equally to the diffraction intensity. Certainly the presence of a large variation in the measured lattice strain for the material which received a high level of prior deformation is associated with the internal stress at the length-scale of a grain, as illustrated by grains 1 to 3 in Figure 11.

For the present measurement, the deviation from linearity for each grain family was calculated from the difference between the measured elastic lattice strain and the expected elastic lattice strain, see Figure 6. A negative value of the deviation from linearity for a particular grain family is an indication of yielding within the grain family population. The neutron diffraction technique can measure only the change in slope when a number of grains belonging to the same grain family have yielded.

A crystal plasticity model was developed that considers both elastic and plastic anisotropy of the polycrystalline grains [18]. Each individual grain within a polycrystalline material was regarded as a spherical inclusion in an infinite homogeneous matrix with the average macroscopic properties [21]. The hardening of the material was described based on Lagneborg's dislocation link length model [22]. A full description of the development of this model has been given elsewhere in [18]. By examining the model during in-situ loading, the onset of deviation from linearity corresponded to the onset of yielding in a certain number of grains. The model predicted similar values of the applied stress for the onset of the deviation from linearity in the {220} grain family in both the ST and EXLA conditions, Figure 7. In order to achieve the best prediction to the measured lattice strains, the crystal plasticity model incorporated a certain value of the critical resolved shear stress (CRSS). It has been demonstrated that the value of CRSS played a significant role in influencing the magnitude of the applied stress required to create the onset of deviation from linearity, Figure 7. The CRSS values of 68MPa and 80MPa were used for ST and EXLA conditions, respectively. Thus the deviation from linearity from the in-situ loading provided a measure of microscopic internal resistance within the selected family of grains. But a model is required to infer the absolute value by assuming an appropriate value for the CRSS.

Discontinuous changes in the slope of the {220} grain family are illustrated by arrows in Figure 7. The increase in the elastic lattice strain as a consequence of the change in slope indicates that other grains in the material have yielded sequentially to create an extra elastic strain (misfit strain). This is consistent with the stress-strain state in a particular grain being controlled by the surrounding grains, as illustrated in Figure 11. The measurements also revealed the change in the yield sequence from the stiffest {220} grain family to the most compliant {200} grain family when specimens received a prior deformation at high temperature, as shown by ST specimen 4 in Figure 9 (a) in a comparison with the other ST specimens in Figure 8 (a).

4.3. Macroscopic internal resistance and a refined internal state concept

From the determination of yield strength in the prior deformed specimens, combined with the knowledge of the pre-existing macroscopic internal stress evaluated by Rietveld refinement analysis, the macroscopic internal resistance has

been derived. For the EXLA specimens, loading led to a higher value of internal resistance compared with the no loading condition. Subsequent creep tended to reduce the internal resistance, Table 3. A peak internal resistance occurred in the primary crept EXLA specimen 7, Table 3. The measured internal resistance in EXLA specimens as a function of the total inelastic strain is shown in Figure 12. Both the corrected values and the uncorrected values have been included, see Table 3. These data are compared with the predicted macroscopic internal resistance based on the evolution of dislocation density as a result of high temperature inelastic deformation. The measured macroscopic internal resistance (i.e. corrected values) in general follows the prediction based on dislocation density, Figure 12. The inserted figure shows the change of dislocation density during inelastic deformation. The change of the dislocation density was measured by Kassner [23] in a face-centred-cubic aluminium. In addition, the initial value of the internal resistance represents the material condition without the presence of dislocation induced hardening, Figure 12.

Kassner [23] suggested a relationship between the macroscopic internal resistance and dislocation density, given by:

$$\sigma_{ir} = \sigma_0 + \alpha M G b \rho^{1/2} \quad (5)$$

where σ_{ir} is the macroscopic internal resistance at a given temperature and strain rate, α is a dimensionless constant describing the strength of a dislocation node, G is the shear modulus, b is the length of Burger's vector, ρ is the dislocation density and M is the Taylor factor, which has a value of 3.06 for polycrystals. σ_0 is the stress required to move a dislocation in the absence of other dislocations that can arise from the presence of solute atoms, Peierls-type stresses and grain size strengthening [23]. The shear modulus at 300K is equal to $8.1 \times 10^{10} \text{ N/m}^2$ and the length of the Burgers vector is equal to $2.58 \times 10^{-10} \text{ m}$ for austenitic stainless steel [24]. For $\alpha=3$ and $\sigma_0=142 \text{ MPa}$, we obtained the best fit to the measured macroscopic internal resistance, Figure 12. Both aluminium and Type 304 stainless steel are classified as the category of pure metal and Class M creep alloys [23], since they have a similar primary creep transient response. Generally during primary creep of a pure metal and the Class M alloys, the dislocation density increases from the initial value to a peak value, but then gradually decreases to a steady state value that is between the initial dislocation density and the

peak density [25] (e.g. Figure 12). This is consistent with the work undertaken by Orlova et al.[26], which demonstrated that the presence of a high value of internal resistance was associated with the loading stage in a creep test.

The Kocks-Mecking (KM) model which follows the general form of equation 1 takes into account the threshold strength to describe inelastic deformation [8, 14]. The threshold strength takes the meaning of internal resistance term in the present paper. In the KM model, the description of the evolution of internal resistance, equation 2, determines the strain rate change in a creep test. Although an attempt was made by Follansbee and Kocks [8] to validate the model predictions, the measured internal resistance at a given strain rate and temperature always gave an increasing value with the increase in inelastic strain. The presently measured macroscopic internal resistance using the incremental deformation combined with neutron diffraction provides a “genuine measure” of the macroscopic internal resistance, by taking into account the presence of macroscopic internal stress. Although only three prior deformed conditions have been considered, a good agreement between the measured internal resistance and the prediction based on the evolution of dislocation density can be found in Figure 12.

Two parameters that identify material internal state have been quantified; internal stress and internal resistance. These two terms are treated separately when describing the inelastic deformation of polycrystalline material, equation 1. Thermal ageing led to a change in material internal resistance and thus the establishment of internal stress would be different when the material was subjected to the same loading history, i.e. loading or period of time over creep, Figure 4. The most appropriate way to consider this effect is based on the total inelastic strain, rather than the period of time spent to reach a specific condition.

5. Conclusions

In-situ neutron diffraction combined with the incremental deformation at room temperature has been applied to study the evolution of the internal stress and internal resistance generated by prior deformation in a face-centred-cubic polycrystalline austenitic stainless steel. The conclusions of this study are:

- I. In-situ neutron diffraction measures a stress-strain response averaged over several similarly orientated grains. However, grain-to-grain interactions

become important when the material has been subjected to a prior deformation and this leads to large variations in the measured lattice strain.

- II. The intergranular internal stress is dependent on specific crystallographic planes and the magnitude is a function of total inelastic strain accumulated in the material.
- III. The deviation from linearity provides a measure of microscopic internal resistance in selected grain families. This has been validated by invoking a crystal plasticity model. In addition, a model is needed to infer the absolute value of microscopic internal resistance by giving an appropriate value of critical resolved shear stress.
- IV. The macroscopic internal resistance after taking into account the presence of the macroscopic internal stress is consistent with the model prediction based on the changes in dislocation density.

Acknowledgements

BC and JNH are grateful to EDF Energy for their financial support. DJS was supported by the Royal Academy of Engineering, EDF Energy and Rolls Royce plc. Mr Yi Qiang Wang made contributions to the neutron diffraction measurements.

References

- [1] Ennis PJ, Zielinska-Lipiec A, Wachter O, Czyrska-Filemonowicz A, *Acta Mater* 1997;45:4901.
- [2] Weiss B, Stickler R, *Metall. Trans.* 1972;3:851.
- [3] Chen B, Flewitt PEJ, Smith DJ, *Mater. Sci. Eng. A* 2010;527:7387.
- [4] Clausen B, Lorentzen T, Leffers T, *Acta Mater* 1998;46:3087.
- [5] Wood WA, Dewsnap N, *Nature* 1948;161:682.
- [6] Chen B, Flewitt PEJ, Cocks ACF, Smith DJ, *Int. Mater. Rev.* 2013 (to be published);
- [7] Taylor GI, *Proc. Roy. Soc.* 1934;145:362.
- [8] Follansbee PS, Kocks UF, *Acta Metall.* 1988;36:81.
- [9] Lund RW, Nix WD, *Acta Metall.* 1976;24:469.
- [10] Hutchinson JW, *Proc. Roy. Soc. Lond. A* 1976;348:101.
- [11] Daymond MR, Bouchard PJ, *Metall. Mater. Trans. A* 2006;37:1863.
- [12] Biberger M, Gibeling JC, *Acta Metall. Mater.* 1995;43:3247.
- [13] Endo T, Shimada T, Langdon TG, *Acta Metall.* 1984;32:1991.
- [14] Estrin Y, Mecking H, *Acta Metall.* 1984;32:57.
- [15] Kocks UF, Mecking H, *Prog. Mater. Sci.* 2003;48:171.
- [16] Santisteban JR, Daymond MR, James JA, Edwards L, *J. Appl. Cryst.* 2006;39:812.
- [17] Daymond MR, Bourke MAM, Von Dreele RB, Clausen B, Lorentzen T, *J. Appl. Phys.* 1997;82:1554.
- [18] Hu JN, Chen B, Smith DJ, Cocks ACF, In: 13th Int. Conf. Fract., Beijing, 2013.
- [19] Dye D, Stone HJ, Reed RC, *Acta Mater* 2001;49:1271.
- [20] Hutchinson JW, *Proc. Roy. Soc. A* 1970;319:247.
- [21] Kroner E, *Acta Metall.* 1961;9:155.
- [22] Lagneborg R, Forsen BH, *Acta Metall.* 1973;21:781.
- [23] Kassner ME, *Acta Mater* 2004;52:1.
- [24] Frost HJ, Ashby MF, *Deformation-mechanism Maps*, Pergamon, Exeter, 1982.
- [25] Clauer AH, Wilcox BA, Hirth JP, *Acta Metall.* 1970;18:381.
- [26] Orlova A, Milicka K, Dobes F, *Mater. Sci. Eng. A* 1995;194:9.

Figure Captions

- Figure 1 A typical deformation history applied to the specimen strained to a primary creep stage, followed by the room temperature incremental tensile deformation: (a) strain history and (b) stress cycles used in the incremental tensile deformation at room temperature combined with neutron diffraction measurement.
- Figure 2 Arrangement of the specimen in the ENGIN-X neutron diffractometer to measure the lattice strains along both axial and radial directions.
- Figure 3 Prior high temperature deformation applied to specimen 4 (ST) and specimen 8 (EXLA): (a) time-independent stress-strain relationship; (b) time-dependent stress-strain relationship together with the creep strain.
- Figure 4 Axial internal stresses due to prior high temperature deformation of ST and EXLA specimens, as a function of total inelastic true strain accumulated at high temperature. A typical error in measurement is given. Numbers correspond to the specimen ID given in Table 2.
- Figure 5 Macroscopic stress-strain relationship during the in-situ loading of specimen 1A.
- Figure 6 Elastic lattice strains along the axial direction for ST specimens 1A, 1B and 1C, which received no prior deformation at high temperature: (a) $\{200\}$ and $\{220\}$ grain families; (b) $\{111\}$ and $\{311\}$ grain families. The predicted elastic lattice strains were obtained from the corresponding diffraction elastic constants (DECs), see the solid lines.
- Figure 7 Influence of the thermal ageing on the subsequent elastic lattice strain response to the stress applied in ST specimen 1A and EXLA specimen 5, where the measured elastic lattice strain in the $\{200\}$ and the $\{220\}$ grain families is compared with a prediction based on a plasticity model [18]. The indicated arrows depicts the discontinuous change in the slope of the $\{220\}$ grain family.
- Figure 8 Influence of the prior creep deformation on the determined deviation from linearity in the $\{220\}$ grain family based on the measurements along the axial direction of the in-situ loaded specimens: (a) ST specimens 1 (1A, 1B, 1C) to 4; (b) EXLA specimens 5 to 8.
- Figure 9 Influence of the prior creep deformation on the determined deviation from

linearity in the $\{200\}$ grain family based on the measurements along the axial direction of the in-situ loaded specimens: (a) ST specimens 1 (1A, 1B, 1C) to 4; (b) EXLA specimens 5 to 8.

Figure 10 Illustration of the determination of the microscopic internal resistances in prior creep deformed specimens from the regression fit obtained deviation from linearity: (a) $\{220\}$ grain family in EXLA specimens 5 and 8 and (b) $\{200\}$ grain family in EXLA specimens 5 and 8.

Figure 11 Arrangement of individual grains (grains 1, 2 and 3) which exhibit the same crystallographic orientation in a locally heterogeneous polycrystal (polycrystals I, II and III), which is embedded into a global homogeneous polycrystal where an external stress, σ_a , is applied to the material.

Figure 12 The measured internal resistance in prior crept EXLA Type 316H stainless steel is compared with the predicted internal resistance based on the evolution of dislocation density in prior crept aluminium [23]. Note: both of the materials are within the same creep category of pure metal and Class M alloy and the initial value of the internal resistance is a function of σ_0 .

Figure 1 (a)
[Click here to download high resolution image](#)

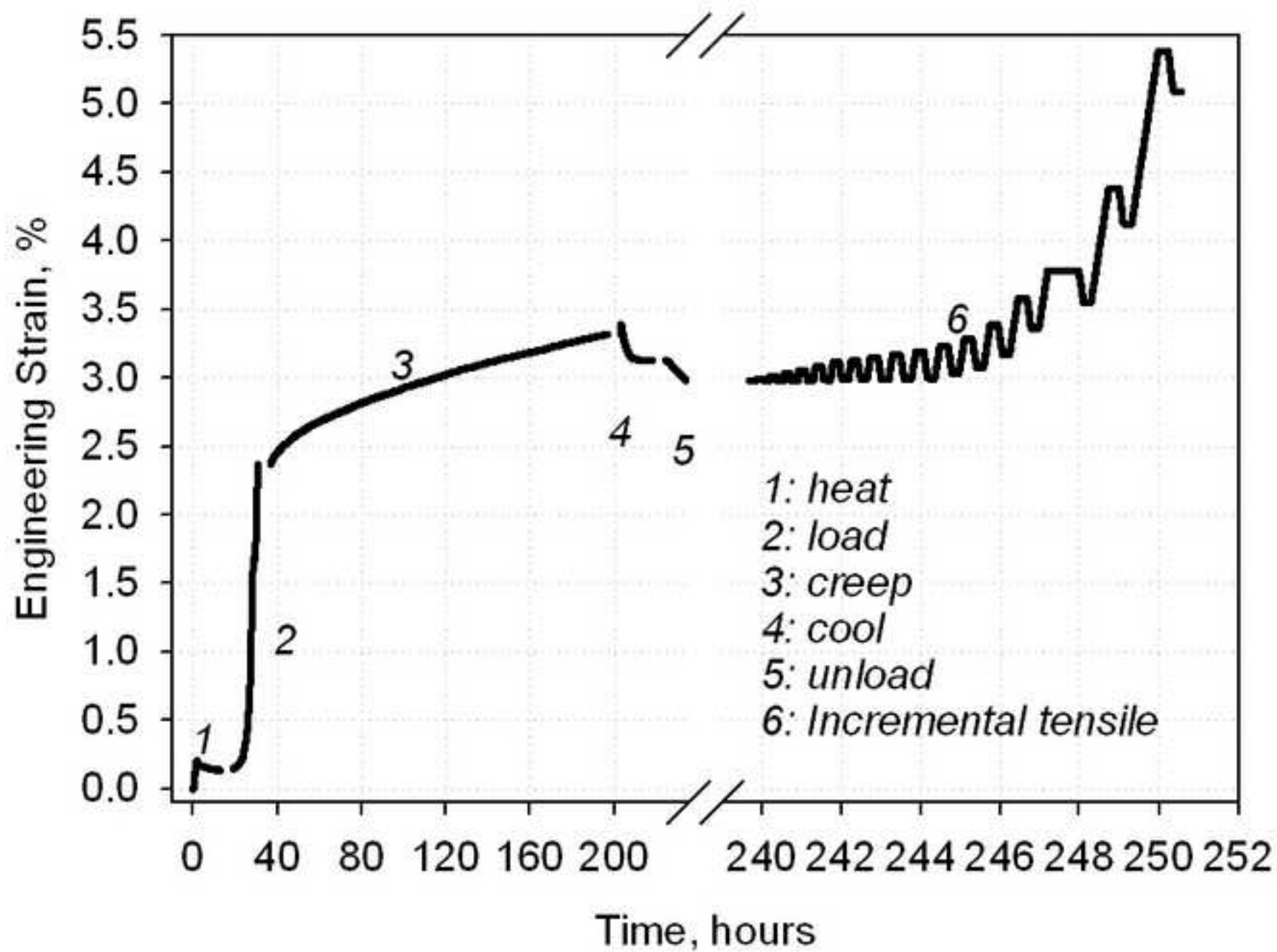


Figure 1 (b)
[Click here to download high resolution image](#)

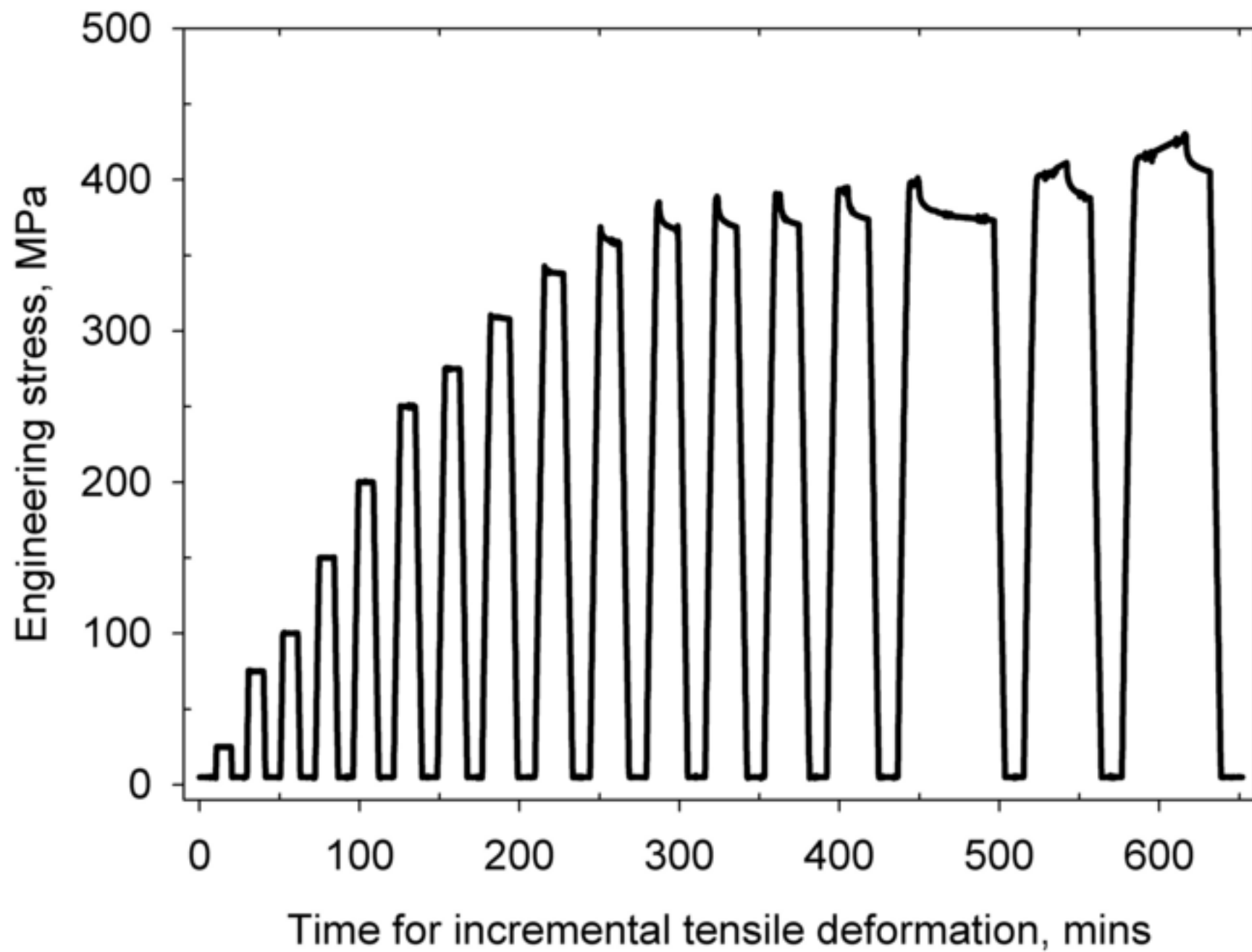


Figure 2
[Click here to download high resolution image](#)

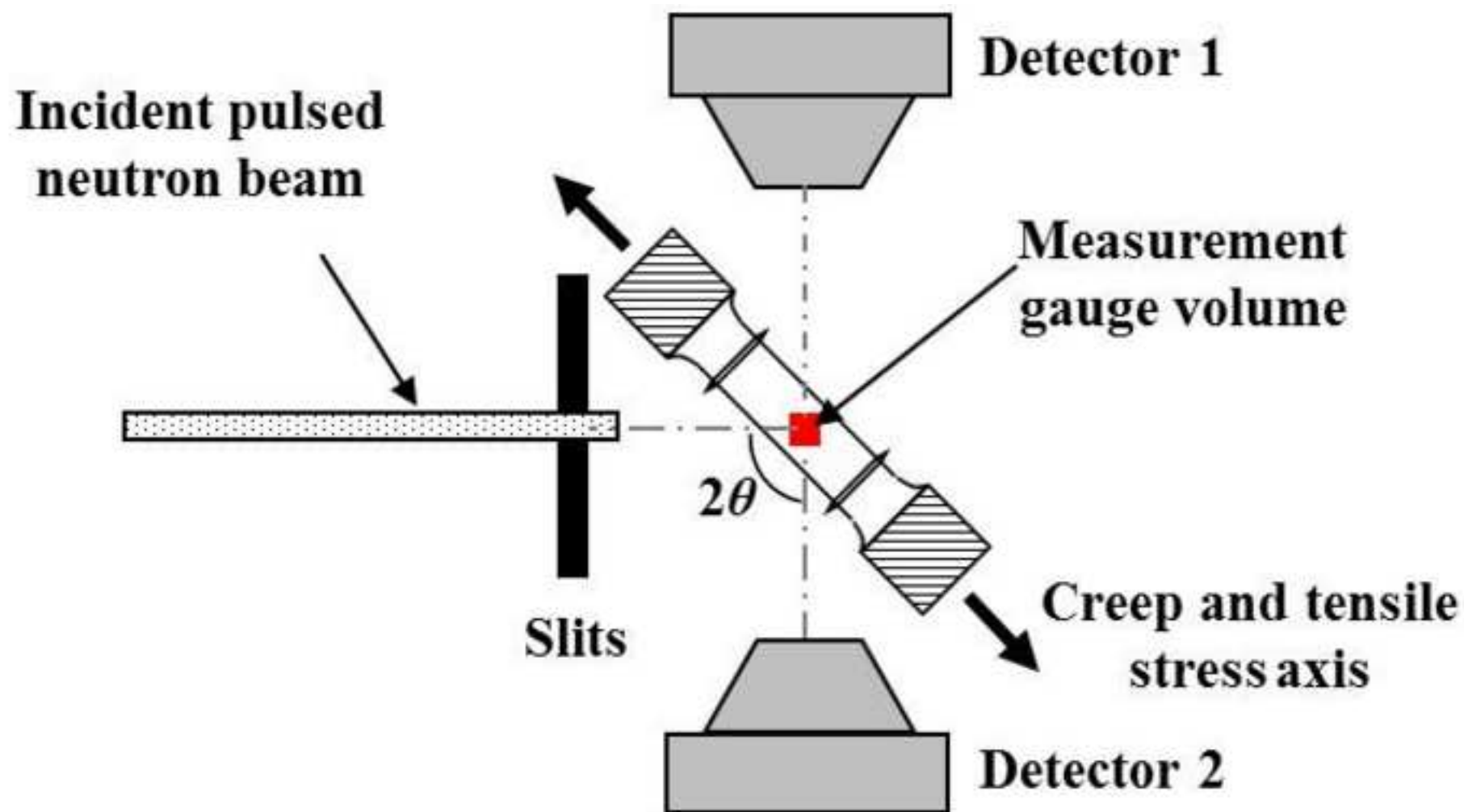
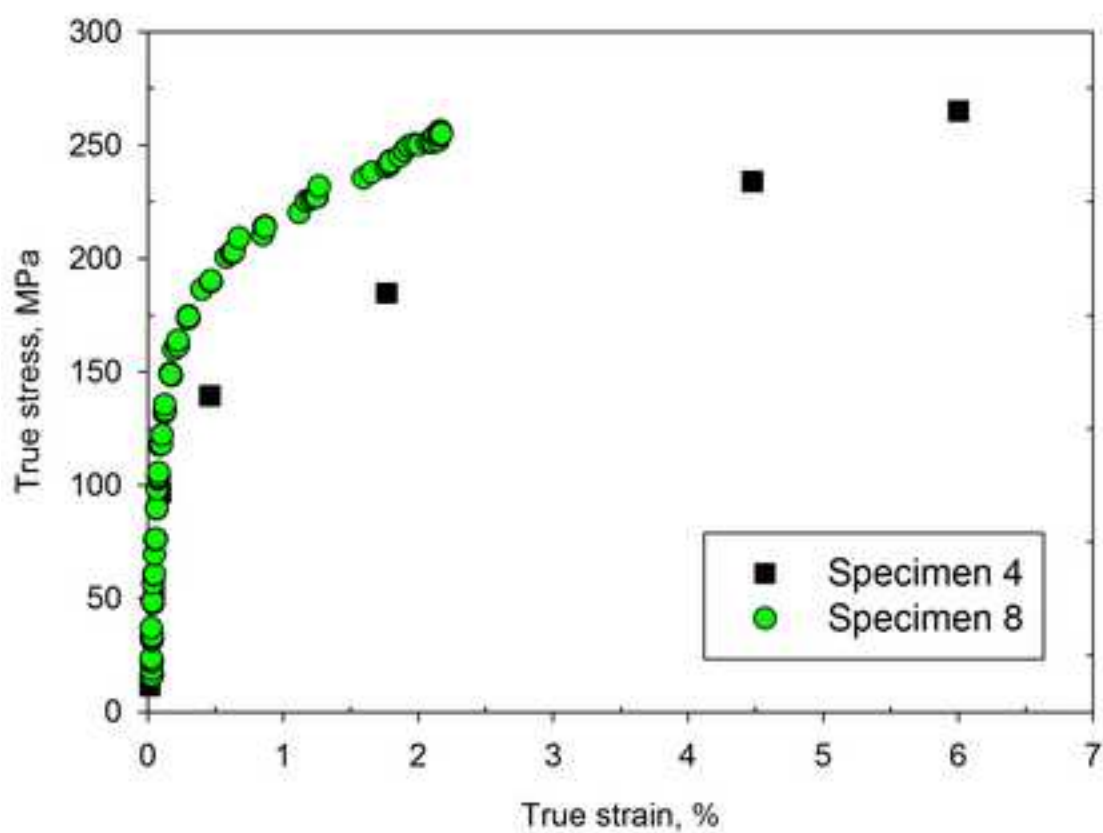
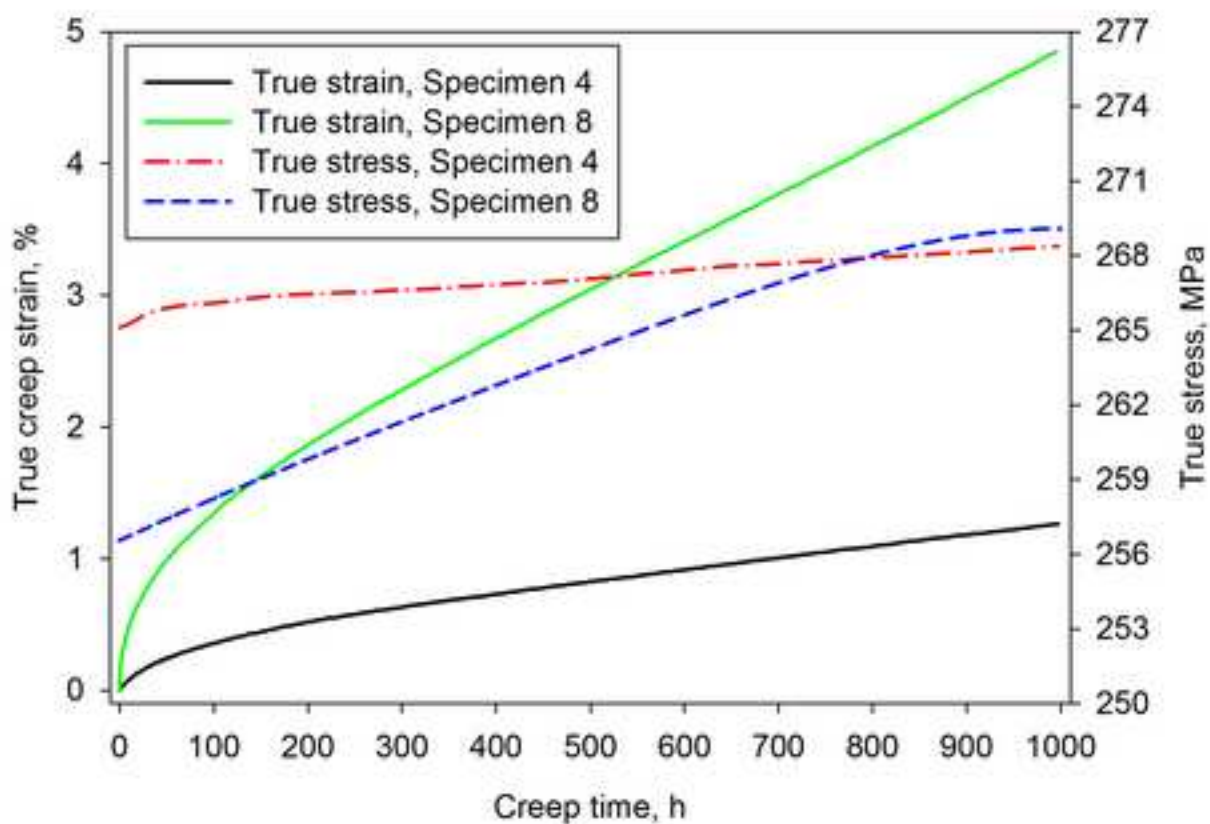


Figure 3
[Click here to download high resolution image](#)



(a)



(b)

Figure 4
[Click here to download high resolution image](#)

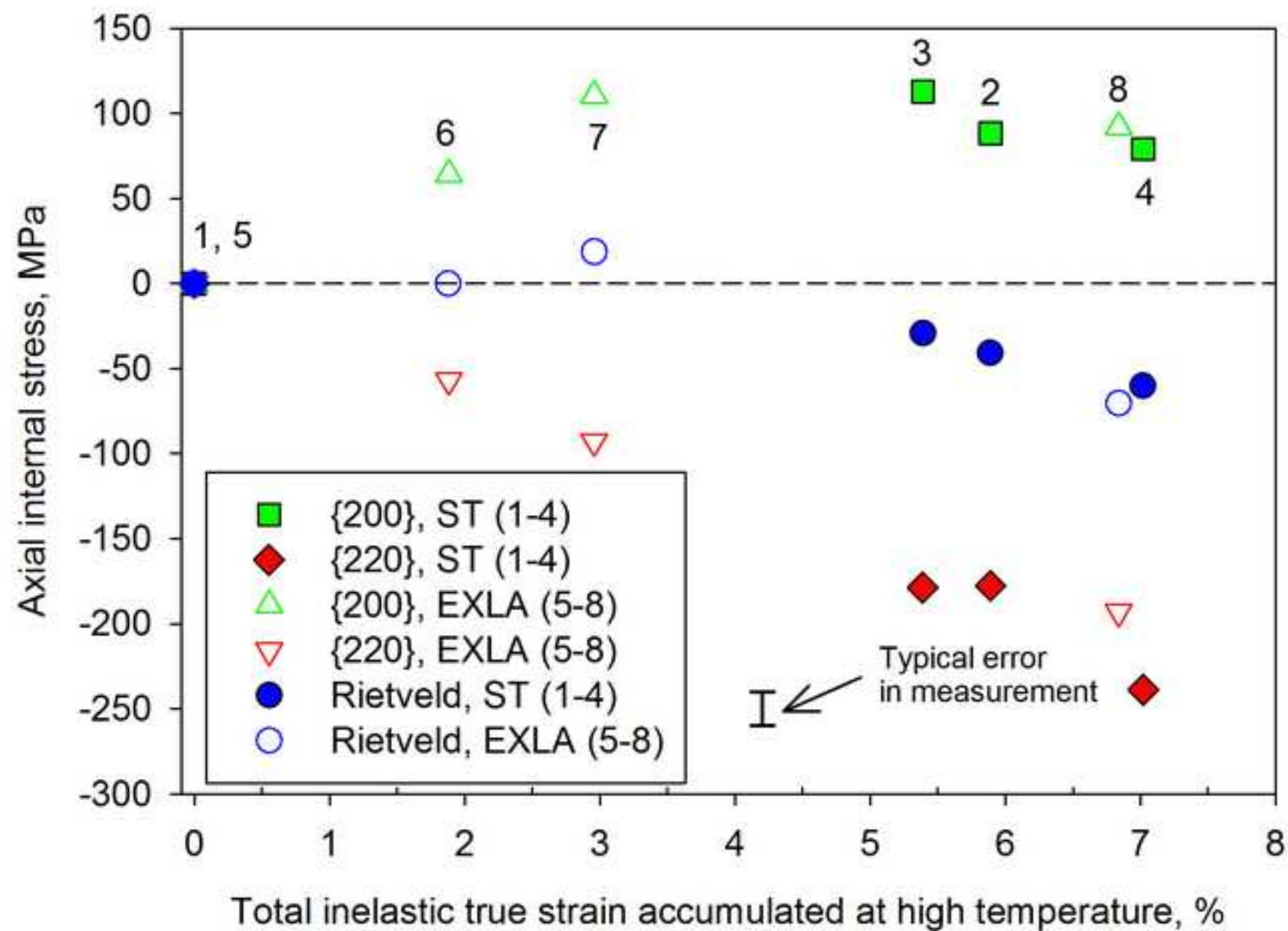


Figure 5
[Click here to download high resolution image](#)

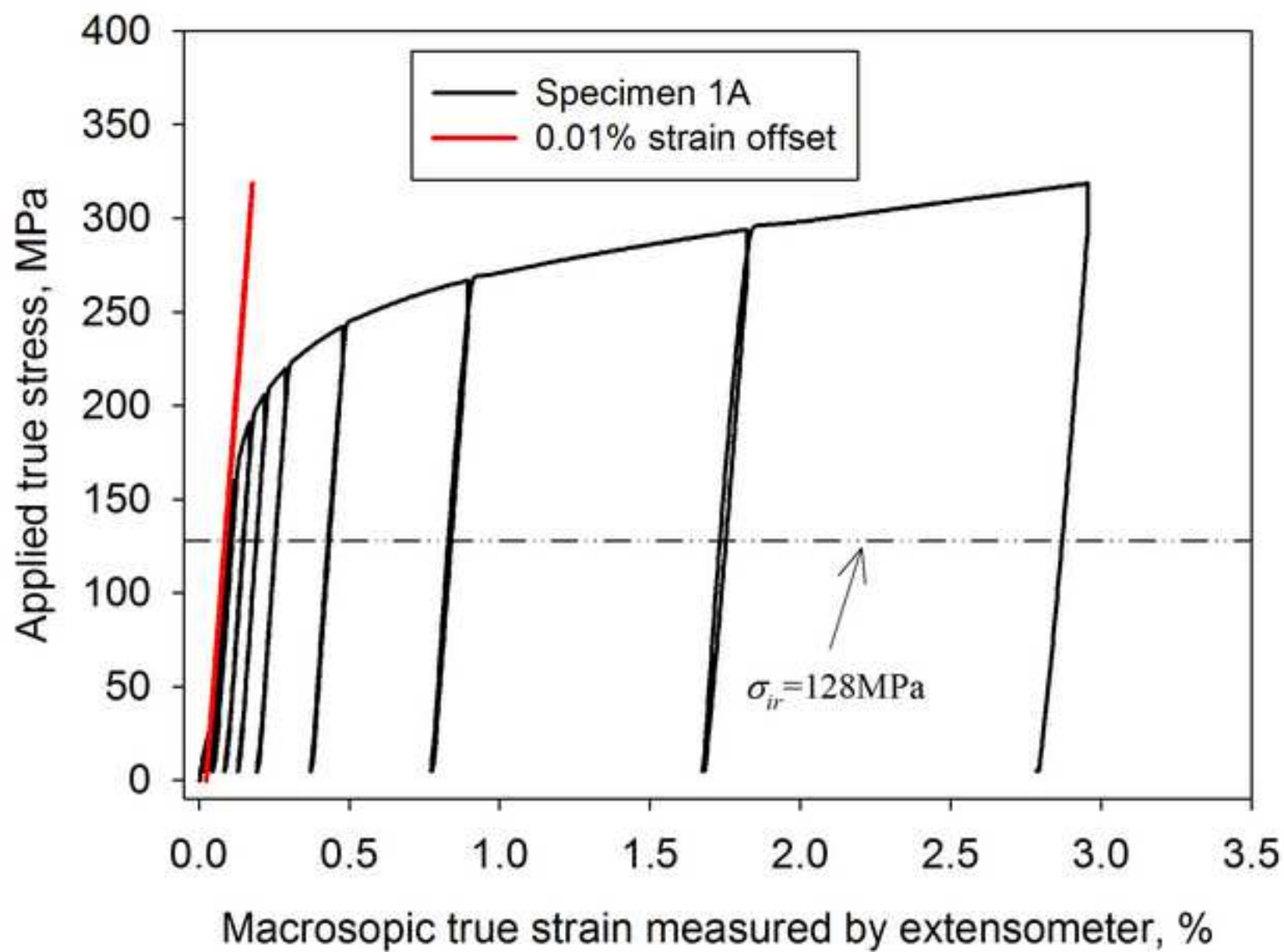
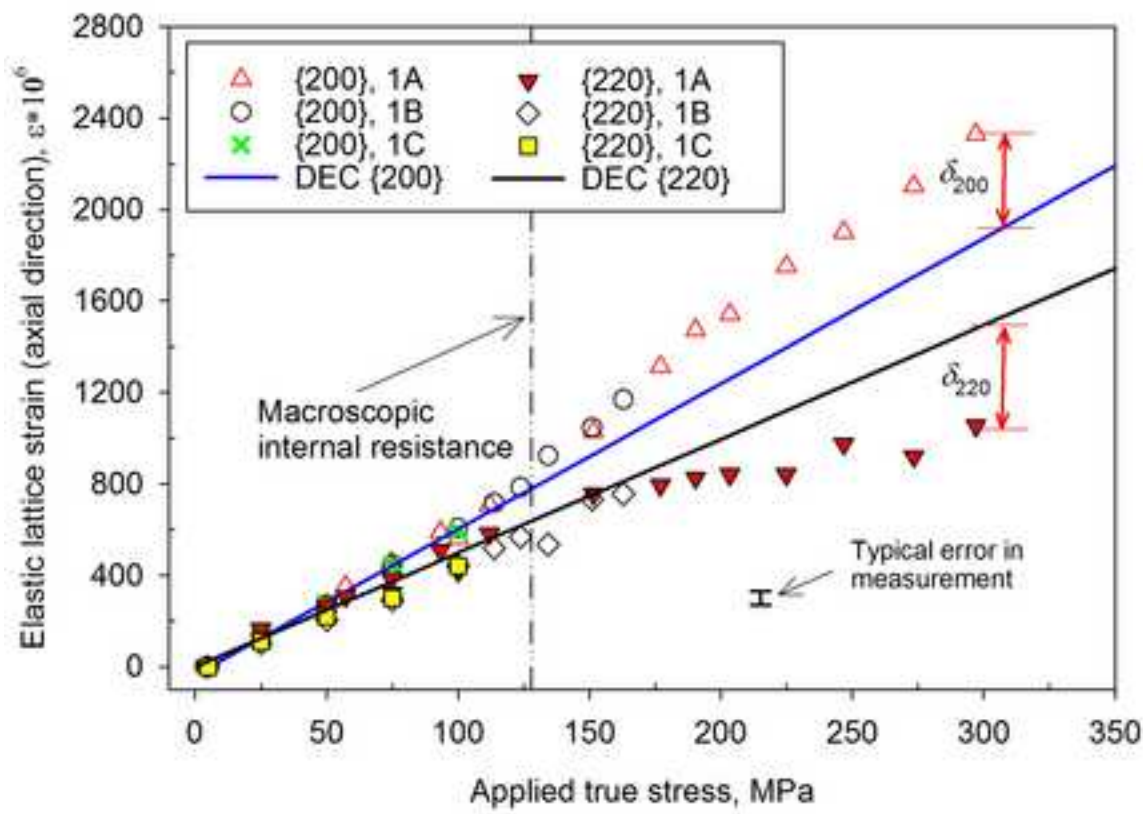
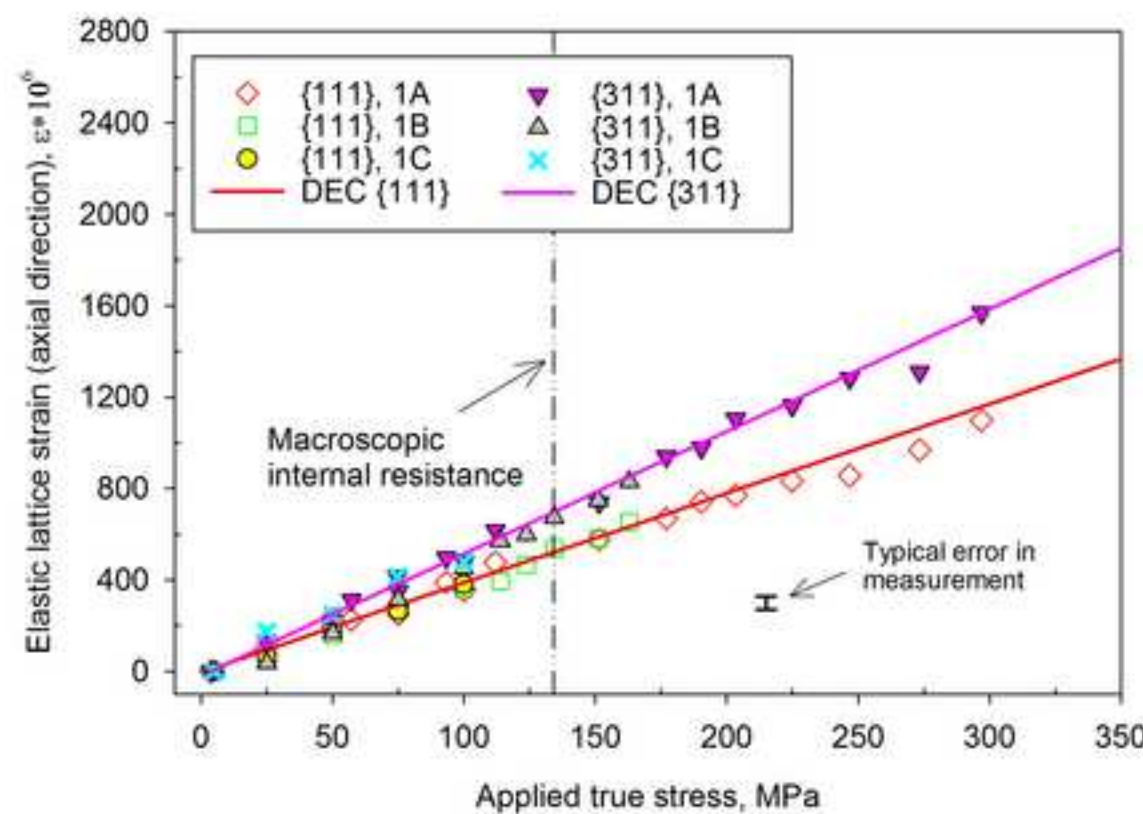


Figure 6
[Click here to download high resolution image](#)



(a)



(b)

Figure 7
[Click here to download high resolution image](#)

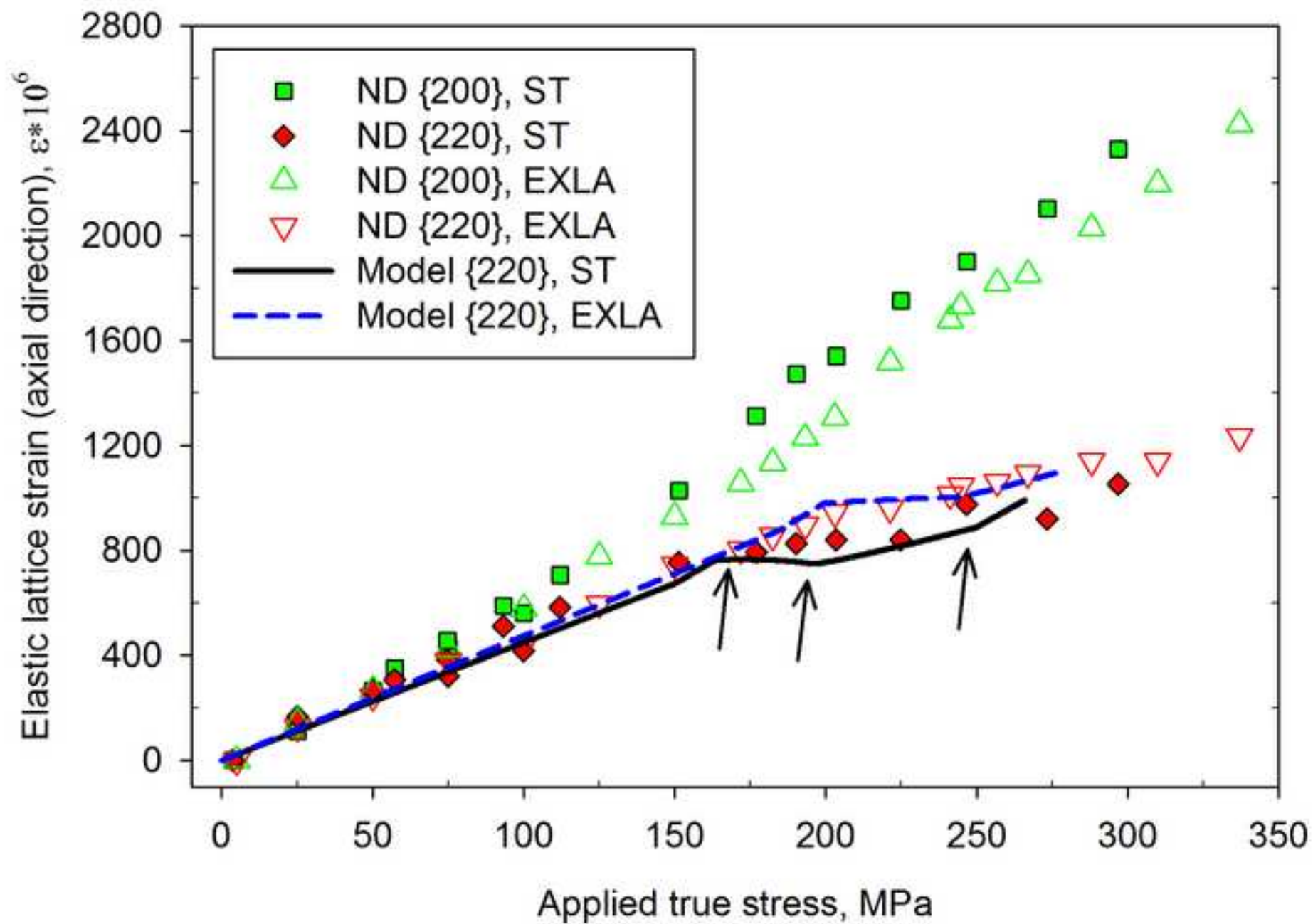
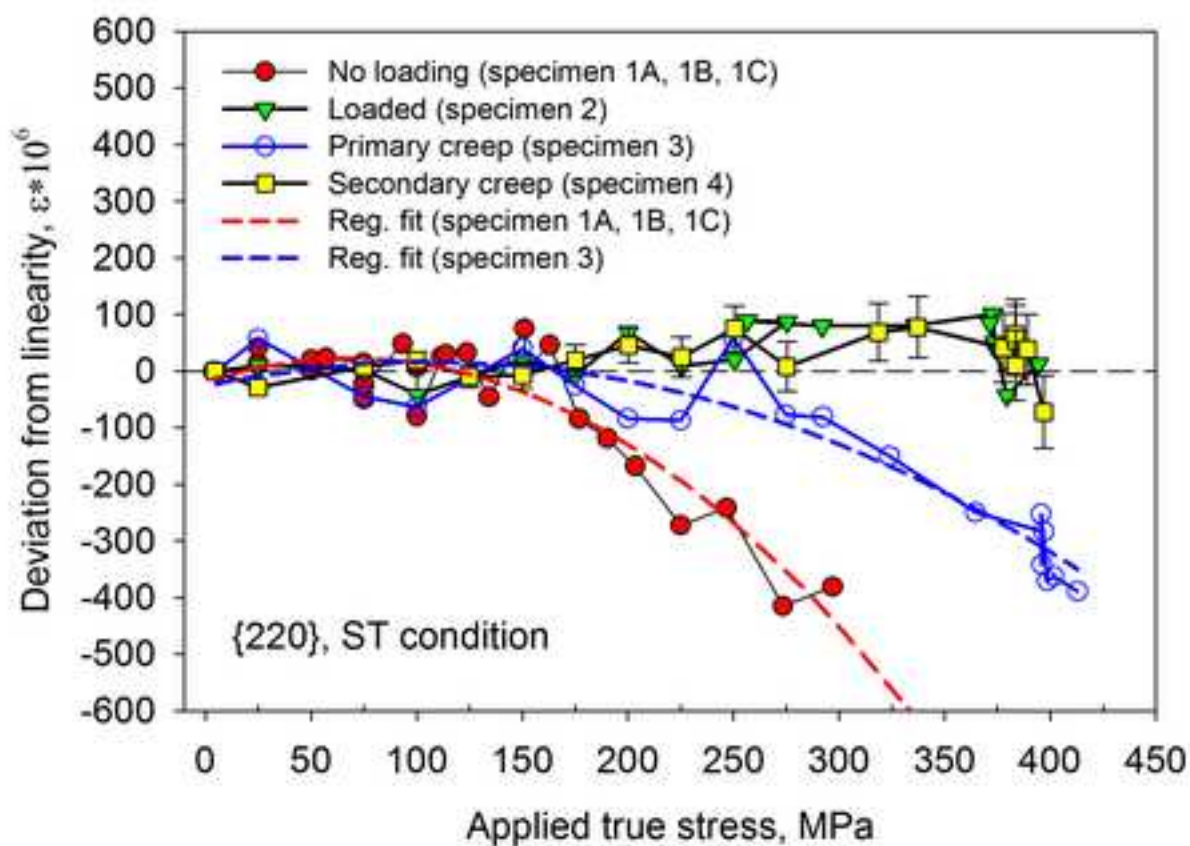
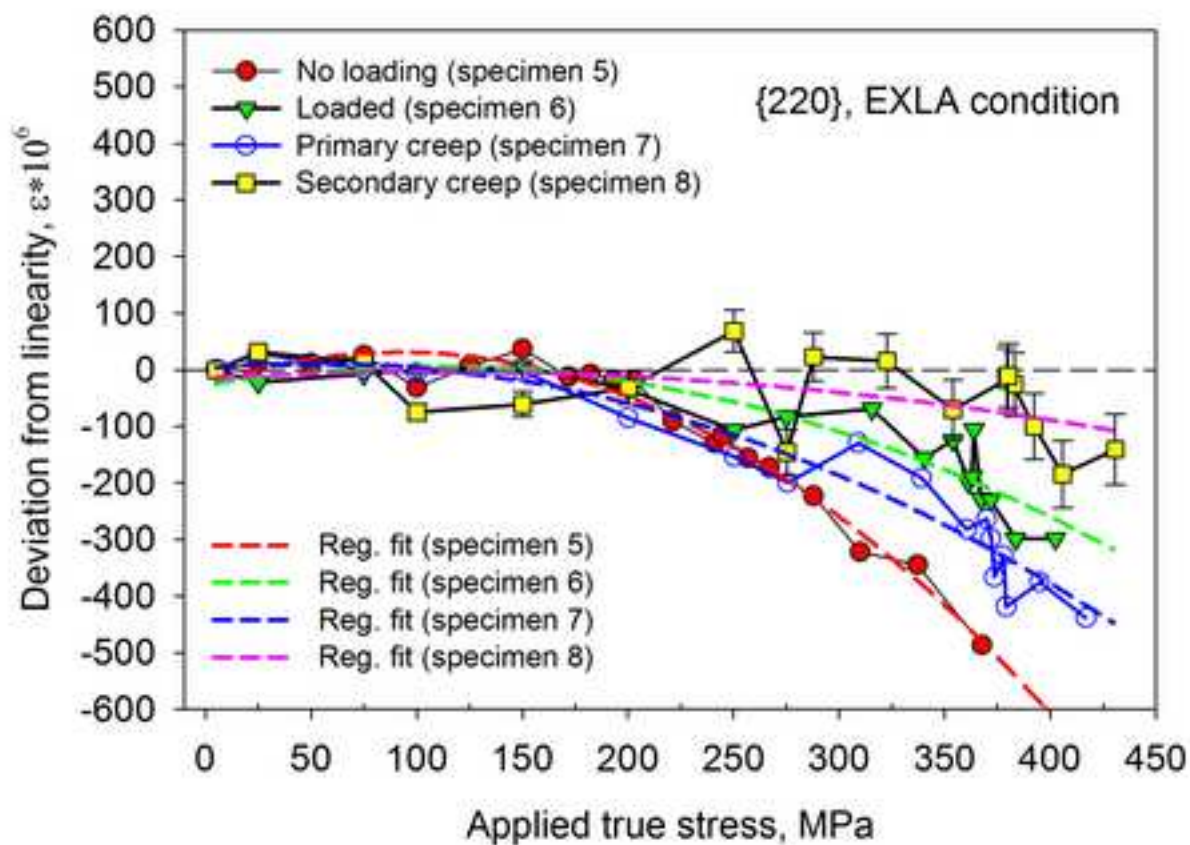


Figure 8

[Click here to download high resolution image](#)



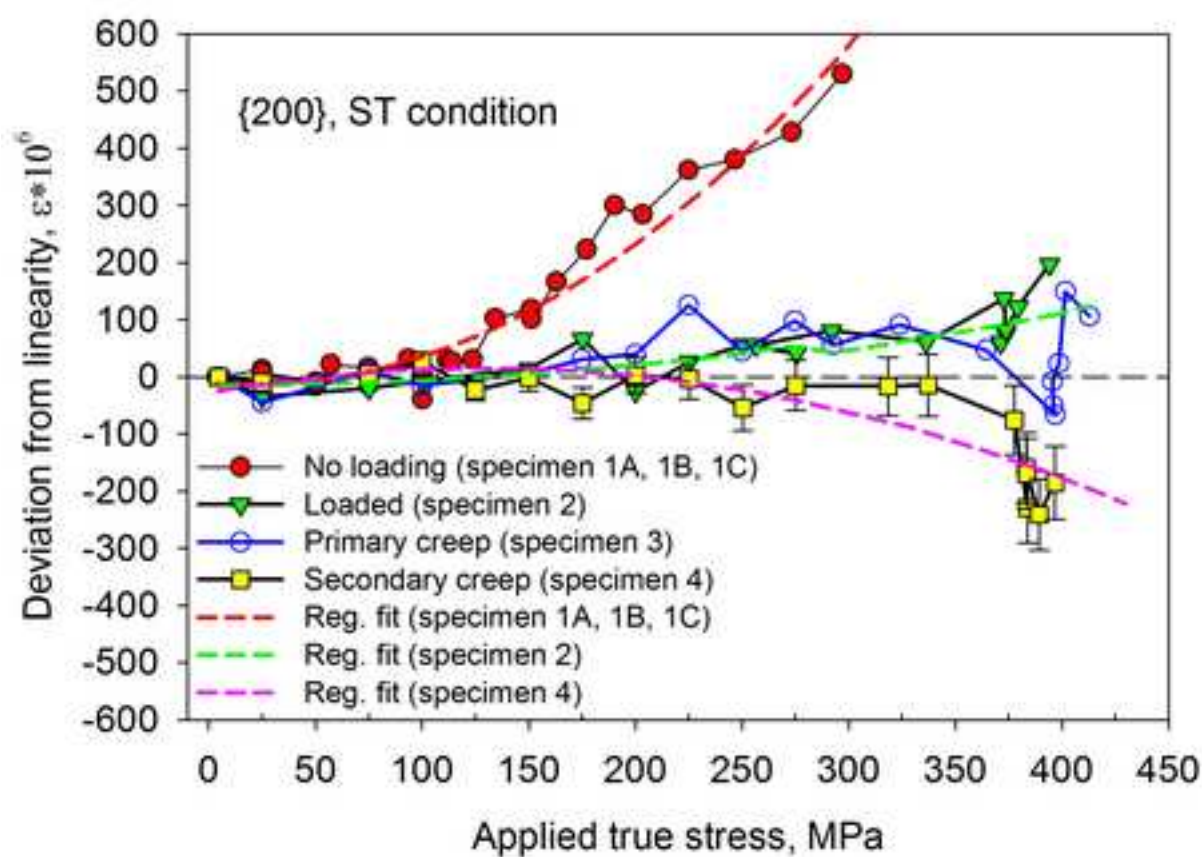
(a)



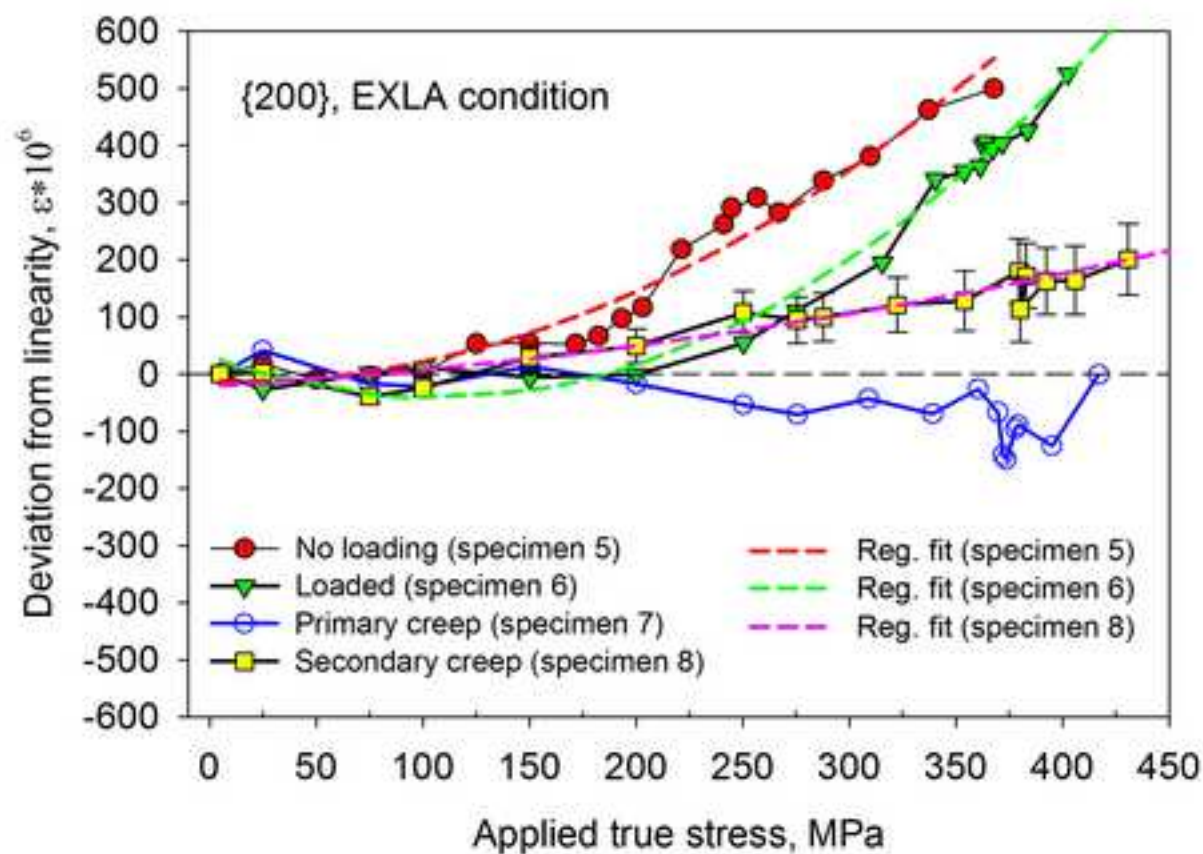
(b)

Figure 9

[Click here to download high resolution image](#)



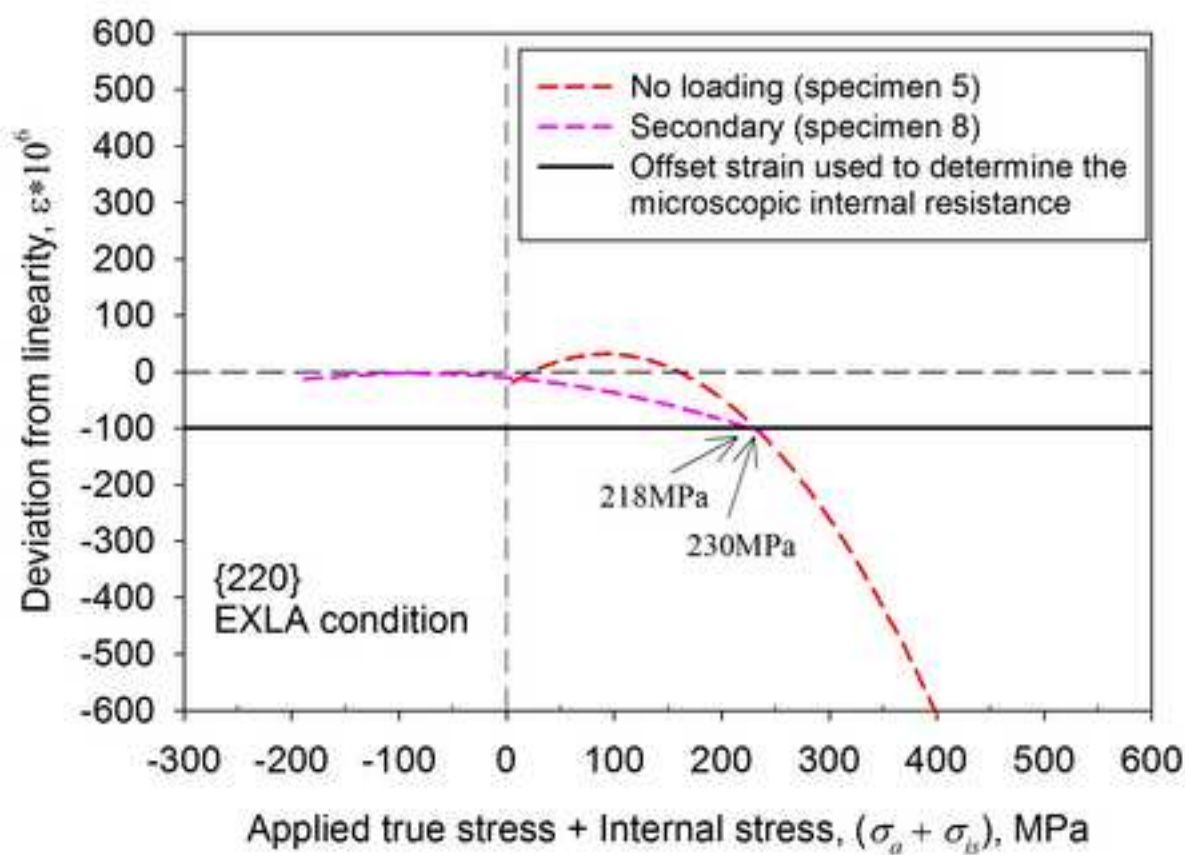
(a)



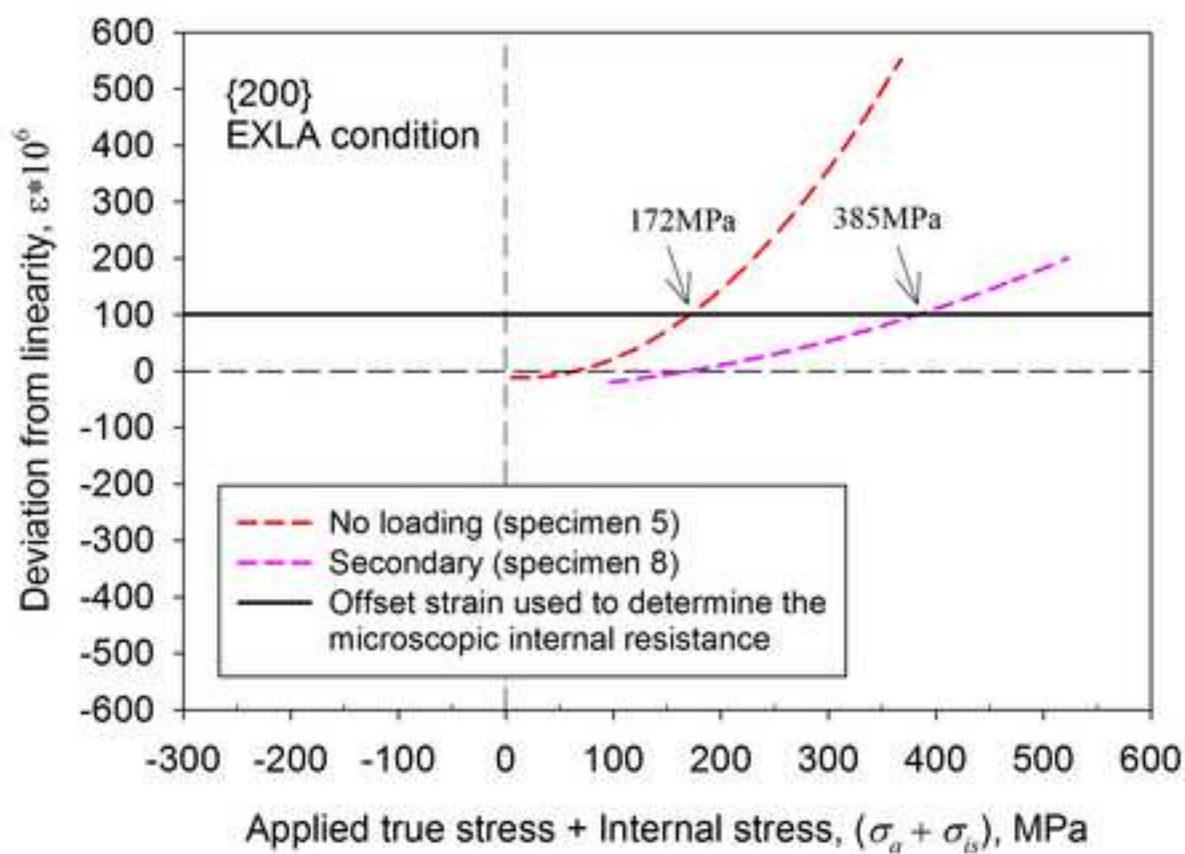
(b)

Figure 10

[Click here to download high resolution image](#)



(a)



(b)

Figure 11
[Click here to download high resolution image](#)

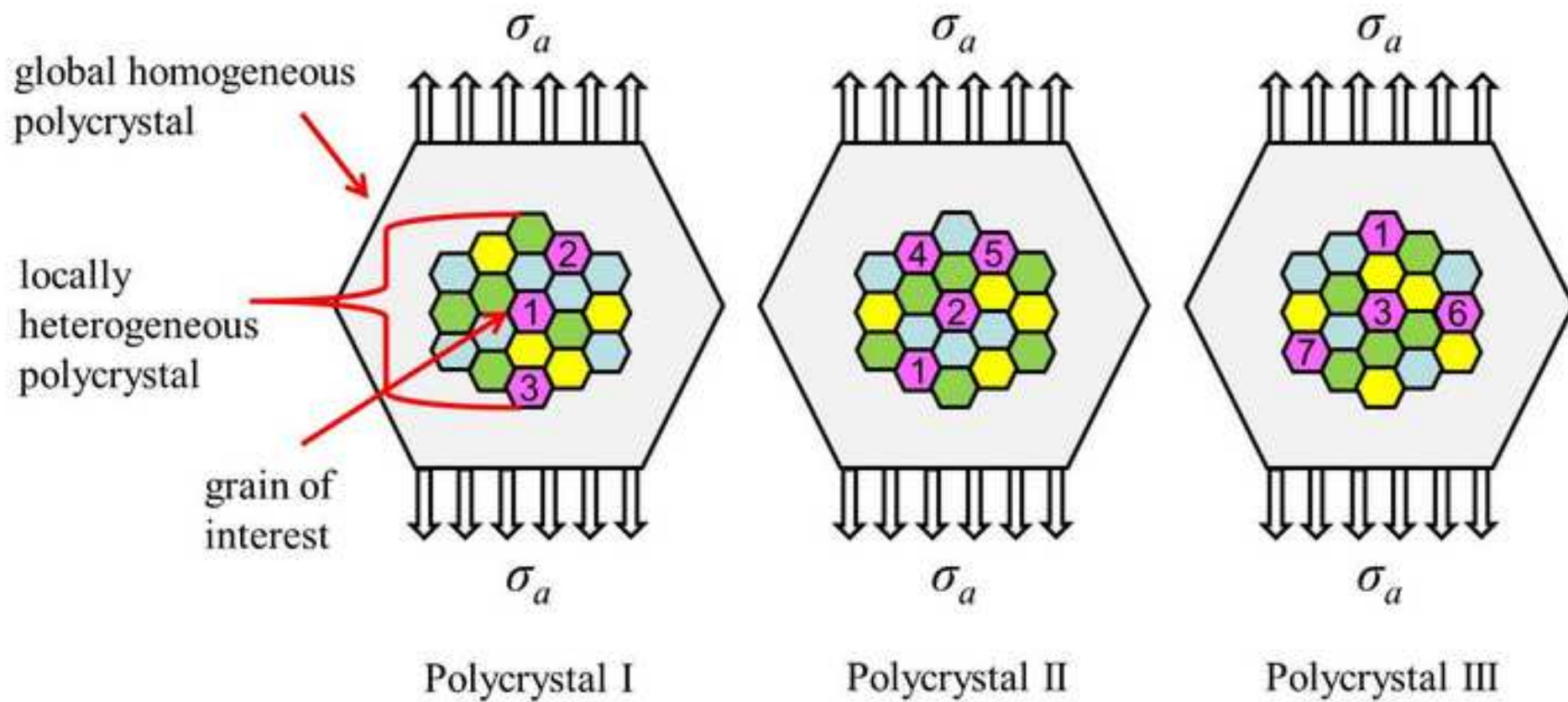
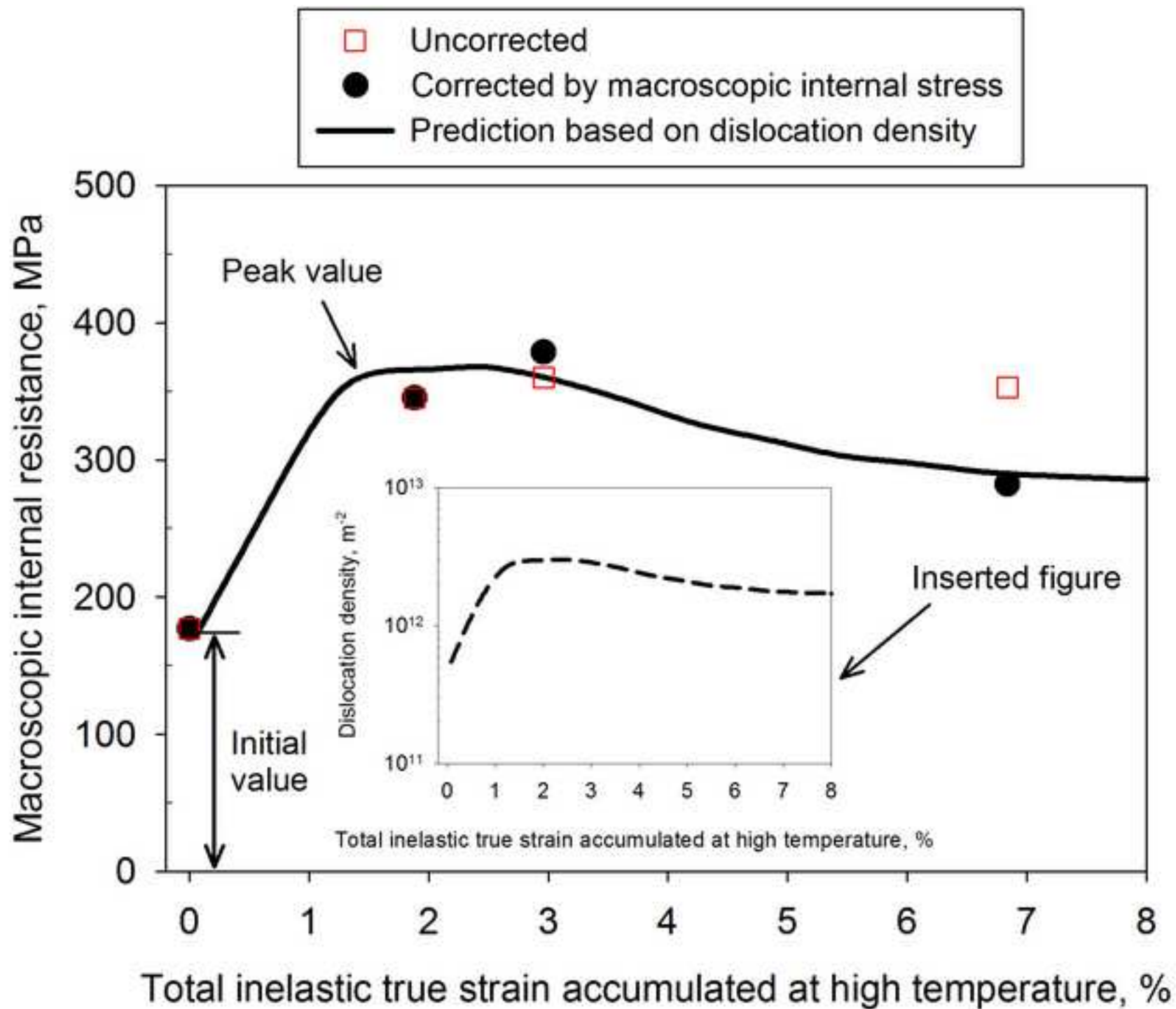


Figure 12
[Click here to download high resolution image](#)



Tables

Table 1. Chemical composition (wt.%) of Type 316H stainless steel

C	Si	Mn	P	S	Cr	Mo	Ni	Co	B	Fe
0.06	0.4	1.98	0.021	0.014	17.17	2.19	11.83	0.10	0.005	Bal.

Table 2. Summary of specimens subject to a prior deformation at high temperature

Specimen ID	Material condition	Prior deformation	Plastic strain, %	Creep strain, %
1 (1A, 1B, 1C)	Solution heat treated (ST)	No loading	0	0
2		Loaded	5.89	0
3		Primary creep	5.12	0.27
4		Secondary creep	5.76	1.26
5	Thermally aged (EXLA)	No loading	0	0
6		Loaded	1.88	0
7		Primary creep	2.04	0.92
8		Secondary creep	1.98	4.86

Table 3. Summary of macroscopic internal resistances

Specimen ID	Material condition	Prior deformation	Macroscopic internal resistance, MPa	
			Uncorrected	Corrected by Rietveld refinement
1A	ST	No loading	128	128
2		Loaded	336	296
3		Primary creep	324	295
4		Secondary creep	360	300
5	EXLA	No loading	177	177
6		Loaded	345	345
7		Primary creep	360	378
8		Secondary creep	353	283

Table 4. Summary of diffraction elastic constants (DECs) obtained from the prior creep deformed ST and EXLA specimens, compared with the previous values given by Clausen et al. [4]

Specimen ID	E_{111}	E_{200}	E_{220}	E_{311}
Specimen1 (1A, 1B, 1C)	254±10	156±3	207±11	186±10
Specimens 1 to 4 (ST)	254±6	158±4	211±8	184±7
Specimens 5 to 8 (EXLA)	253±10	155±6	213±10	184±11
Previously measured [4]	261.3	155.0	222.3	192.6

Table 5. Summary of microscopic internal resistances determined from the deviations from linearity in the {220} and the {200} grain families for both ST and EXLA specimens

Specimen ID	Material condition	Prior deformation	Microscopic internal resistance after taking into account the intergranular internal stress, MPa	
			{220} grain family	{200} grain family
1 (1A, 1B, 1C)	ST	No loading	187	143
2		Loaded	No deviation	445
3		Primary creep	101	No deviation
4		Secondary creep	No deviation	417
5	EXLA	No loading	230	172
6		Loaded	235	317
7		Primary creep	142	No deviation
8		Secondary creep	218	385